



Endosomal receptor kinetics determine the stability of intracellular growth factor signalling complexes

A. Rami TZAFRIRI* and Elazer R. EDELMAN*†

*Harvard–MIT Division of Health Sciences and Technology, Massachusetts Institute of Technology, Room 16-343, Cambridge, MA 02139, U.S.A., and †Cardiovascular Division, Department of Medicine, Brigham and Women's Hospital, Harvard Medical School, Boston, MA 02115, U.S.A.

There is an emerging paradigm that growth factor signalling continues in the endosome and that cell response to a growth factor is defined by the integration of cell surface and endosomal events. As activated receptors in the endosome are exposed to a different set of binding partners, they probably elicit differential signals compared with when they are at the cell surface. As such, complete appreciation of growth factor signalling requires understanding of growth factor–receptor binding and trafficking kinetics both at the cell surface and in endosomes. Growth factor binding to surface receptors is well characterized, and endosomal binding is assumed to follow surface kinetics if one accounts for changes in pH. Yet, specific binding kinetics within the endosome has not been examined in detail. To parse the factors governing the binding state of endosomal receptors we analysed a whole-cell mathematical model of epidermal growth factor receptor trafficking and binding. We discovered that the

stability of growth factor–receptor complexes within endosomes is governed by three primary independent factors: the endosomal dissociation constant, total endosomal volume and the number of endosomal receptors. These factors were combined into a single dimensionless parameter that determines the endosomal binding state of the growth factor–receptor complex and can distinguish different growth factors from each other and different cell states. Our findings indicate that growth factor binding within endosomal compartments cannot be appreciated solely on the basis of the pH-dependence of the dissociation constant and that the concentration of receptors in the endosomal compartment must also be considered.

Key words: intracellular binding, mathematical modelling, quasi-steady state approximation, receptor trafficking, systems biology.

INTRODUCTION

Endocytosis enables cells to internalize a diverse set of compounds from serum proteins, to growth factors and viruses [1]. Ligand–receptor complexes formed at the cell surface are transported into common endosomes [2], from which they are sorted to a variety of destinations. The form and nature of the internalized complexes determine their kinetics and fate. Several ligands including, low-density lipoprotein, asialoglycoproteins, α_2 -macroglobulin and lysosomal enzymes dissociate from their receptors within the endosomes prior to delivery of ligand to lysosomes [1]. These compounds fall close to a polar extreme, wherein pronounced dissociation leads to recycling of receptors to the cell surface, where they can re-internalize as part of a new round of endocytosis. Compounds like transferrin represent the other extreme as they do not dissociate from their receptors within endosomes and are recycled together with their receptors [1,3]. Growth factors classically fall in a broad middle-range with a variable balance of recycling and degradation [1]. EGF (epidermal growth factor) is the conventional model for a growth factor that remains predominantly bound to its receptor, EGFR (EGF receptor), during the major intracellular trafficking steps preceding lysosomal degradation [4,5]. TGF α (transforming growth factor α) on the other hand also binds and activates EGFR, but readily dissociates from its receptor in the sorting endosomes [6–8].

Interest in the stability of intracellular growth factor complexes initially focused on surface receptor down-regulation [6,7]. More recently, it has been established that many internalized growth factor–receptor complexes remain phosphorylated and continue

to signal in the endosome [8–14]. Association of the growth factor to the internalized receptor is a requisite for endosomal signalling. Stability of the internalized complex is thus a crucial factor determining the magnitude and duration of endosomal signalling, and has been invoked to explain the differential signalling elicited by various ligands of EGFR [8,10,15,16]. Moreover, compartmentalization of signalling molecules suggests a differential role for surface and endosomal signalling [8–10,17–20], and implies that surface and endosomal receptors are inter-related complementary targets for growth factor delivery. Classic correlation of biological response with steady-state surface receptor activation [21] is therefore simplistic. Optimization of growth factor presentation kinetics more likely requires the maintenance of an intricate balance between activation of surface and intracellular receptors. Mathematical modelling can be a useful tool for investigating these processes across the broad range of intrinsic and environmental conditions. Since the seminal paper of Wiley and Cunningham [22], kinetic models have augmented and supported the experimental analysis of growth factor trafficking experiments and have contributed to the conceptual understanding of these processes [20–26].

We examined the factors that govern the stability of endosomal growth factor complexes with a model of EGFR trafficking. All the relevant trafficking parameters including surface and endosomal binding constants have been experimentally estimated using the B82 cell line [23,26]. Surprisingly, simulations of the model using published parameter estimates (Tables 1 and 2) implied that internalized TGF α is predominantly bound (85%) and not dramatically different from the binding state of EGF (93%). These results are insensitive to the magnitude of the endocytosis

Abbreviations used: EGF, epidermal growth factor; EGFR, EGF receptor; IL-2, interleukin 2; PDGF, platelet-derived growth factor; TGF α , transforming growth factor α .

¹ To whom correspondence should be addressed (email ramitz@mit.edu).

Table 1 Constitutive trafficking parameters for EGFR

Constitutive trafficking parameters for EGFR transfected into B82 fibroblasts [23,26,35] and four ligands: EGF, TGF α and the EGF analogs E40A and Y13G [35].

(a) Surface parameters

Parameter	Meaning	Baseline value
k_e^*	Endocytosis rate constant	0.165 min ⁻¹
k_i^\dagger	Constitutive internalization rate constant	0.030 min ⁻¹
n	Cell density	10 ⁸ cells/l
R_{s0}^\dagger	Surface receptor number	118 576/cell

(b) Endosomal parameters

Parameter	Meaning	Baseline value
k_{hr}^\dagger	Receptor degradation rate constant	0.0022 min ⁻¹
k_{nl}^\dagger	Ligand degradation rate constant	0.010 min ⁻¹
k_x^\dagger	Receptor recycling	0.058 min ⁻¹
k_{syn}^\dagger	Receptor synthesis rate	130 receptors/cell min ⁻¹
V_e^\dagger	Total endosomal volume	10 ⁻¹⁴ litres/cell
R_{i0}^\dagger	Endosomal receptor number	59 091/cell

* Average estimates for B82 fibroblasts [23].

† Published estimates for B82 fibroblasts [26].

rate constant, but are sensitive to alterations in the endosomal volume. To define explicit criteria for the stability of internalized ligand complexes, we examined the case with a minimal endocytosis rate constant. Though such an analysis approximates the expected kinetics of receptors that do not appreciably down-regulate [26–28], our modelling validates findings in down-regulating receptors, including EGFR. Constitutively trafficked non-down-regulating receptors follow simple surface binding and internalization kinetics, and are therefore ideal systems for focusing on downstream endosomal interactions. Application of a combination of model reduction techniques [29–31] enabled us to fully characterize the dynamics of endosomal growth factor as a function of ligand load, receptor expression and apparent dissociation constant. We demonstrate that the stability of endosomal complexes is determined by three primary and seemingly independent factors: the endosomal dissociation constant, the total endosomal volume and the number of endosomal receptors. We show further that these factors can perhaps be best appreciated as an integrated force, and when distilled into a single dimensionless parameter uniquely define each growth factor in its application space. More specifically, complex stability is guaranteed whenever the concentration of endosomal receptors greatly exceeds the binding dissociation constant, consistent with standard notions on the

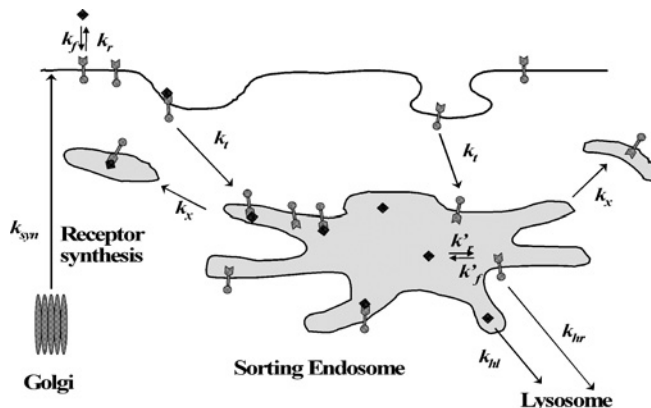
Table 2 Binding rate constants for EGFR

Binding rate constants for EGFR transfected into B82 fibroblasts [23,26,35] and four ligands: EGF, TGF α and the EGF analogs E40A and Y13G [35].

Ligand	Surface receptors*		Endosomal receptors†	
	Binding off rate constant k_r (min ⁻¹)	Equilibrium dissociation constant $K_d \equiv k_r/k_f$ (nM)	Binding off rate constant k_r' (min ⁻¹)	Equilibrium dissociation constant $K_d' \equiv k_r'/k_f'$ (nM)
EGF	0.16	2.5	0.66	78
TGF α	0.27	6.3	2.30	404
E40A	0.41	61	1.75	417
Y13G	1.24	133	1.41	164

* Estimated from EGF binding to B82 fibroblasts at pH 7.4 [35].

† Estimated from EGF binding to B82 fibroblasts at pH 6.0 [35].

**Figure 1** Rate limiting constitutive trafficking steps considered by Starbuck and Lauffenburger [26]

New receptors are continually synthesized in the Golgi and brought to the cell surface at a rate k_{syn} . Surface receptors (round-headed arrows) are internalized constitutively with rate constant k_i . Internalized receptors can either recycle to the surface with rate constant k_x or be sorted to degradation and exocytosis with rate constant k_{hr} . Extracellular ligand (♦) binds reversibly to free surface receptor with on rate k_f and off rate k_r , and does not alter the trafficking of unoccupied receptors. Ligand–receptor complexes (round-headed arrows attached to ♦) are endocytosed with rate constant k_e . Internalized complexes can either recycle to the surface with rate constant k_x or be sorted to degradation and exocytosis with rate constant k_{nl} . This model only considers the rate limiting steps of receptor–ligand trafficking and neglects fast processes such as dimerization of surface receptors, activation of occupied receptors and binding to surface proteins, etc. [23].

thermodynamics of chemical reactions. Our findings imply that stability of intracellular signalling complexes is not an inherent property of the ligand and the receptor, which can be divorced from the intracellular milieu. Rather, it is a systems property, which must be studied in the appropriate context. Receptor complexes would tend to be more stable in cells that overexpress receptors, thereby altering the signalling bias between cell-surface bound and internalized receptors. This may, in part, explain the correlation between receptor overexpression and aberrant intracellular signalling, as indicated by the high incidence of overexpression in tumour derived cells.

THE MODEL

The accepted rate limiting steps in constitutive EGF trafficking [23,26] can be modelled using the following kinetic equations (Figure 1)

Surface species:

$$dR_s/dt = -k_f R_s L_o + k_r C_s - k_i R_s + k_x R_i + k_{syn} \quad (1)$$

$$dC_s/dt = k_f R_s L_o - (k_r + k_e) C_s + k_x C \quad (2)$$

$$(N_A/n)dL_o/dt = -k_f R_s L_o + k_f C_s \quad (3)$$

Intracellular species:

$$dC_i/dt = k_e C_s + k_f R_i L_i - k_f C_i - (k_{hr} + k_x) C_i \quad (4)$$

$$(V_e N_A) dL/dt = -k_f R_i L_i + k_f C_i - k_{hl} (V_e N_A) L_i \quad (5)$$

$$dR_i/dt = -k_f R_i L_i + k_f C_i + k_t R_s - (k_{hr} + k_x) R_i \quad (6)$$

Similar models have been used to model the trafficking of asialoglycoprotein [32], transferrin [3], IL-2 (interleukin 2) [33] and granulocyte colony stimulating factor [34].

ANALYSIS OF LIGAND INTERNALIZATION KINETICS

Ligand internalization is typically studied *in vitro* by exposing homeostatic cells to a bolus of extracellular ligand at 37°C. As such the following initial conditions hold:

$$(R_s, C_s, L_o, C_i, L_i, R_i) = (R_{s0}, 0, L_o, 0, 0, R_{i0}) \quad (7)$$

where R_{s0} and R_{i0} are the surface and internal homeostatic receptor numbers [23]:

$$R_{s0} \equiv (k_{syn}/k_t)(1 + k_x/k_{hr}), R_{i0} \equiv k_{syn}/k_{hr} \quad (8)$$

We simulated eqns (1–7) for 10 nM boluses of four different EGFR agonists (Tables 1 and 2) and plotted the corresponding numbers of internalized complexes, C_i , and total internalized ligand molecules:

$$l_i \equiv (N_A V_e) L_i + C_i \quad (9)$$

Remarkably, all four agonists remain predominantly bound to the EGFR after internalization, (Figure 2A). Such binding is expected for EGF, but surprising for TGF α , E40A and Y13G, which are thought to be predominantly free in the sorting endosomes [35]. Indeed, the EGF analogues E40A and Y13G were specifically designed to have unusually high dissociation constants at pH 6.0. Increasing the basal endocytosis rate constant 2-fold ($k_e = 0.33 \text{ min}^{-1}$) provided for similar endosomal binding patterns: EGF (91%), TGF α (82%), E40A (93%) and Y13G (98%). Decreasing the endocytosis rate constant 5.5-fold to its minimal constitutive value $k_e = k_f = 0.03 \text{ min}^{-1}$ reduced the number of internalized ligand molecules, but did not significantly alter the endosomal binding fractions (Figure 2B). Taken together, these examples suggest that the stability of endosomal complexes is not strongly influenced by the endocytosis rate constant. We therefore focused on a subclass of constitutively internalized receptors [26–28] for which the mathematical analysis is greatly simplified, but explicitly tested the relevance of our results for wild-type EGFR (which are shown in Figure 5 and will be discussed in more detail below).

Eqns (1–6) imply the following conservation laws for constitutively internalized surface complexes:

$$R_s + C_s = R_{s0}, R_i + C_i = R_{i0} \quad (10)$$

This is the mathematical statement that shows that constitutively trafficked receptors do not downregulate. When a negligible fraction of endosomal ligand is free, steady-state is achieved when the clearance rate of bound ligand, $(k_x + k_{hr})C_i$, approximately balances the rate of ligand internalization, $k_f C_s$. Assuming

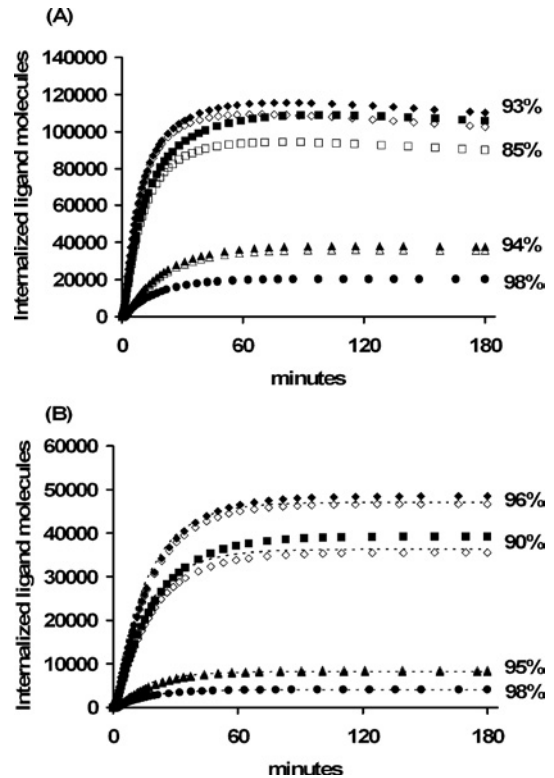


Figure 2 Internalized growth factor following a 10 nM bolus of EGF (diamonds), TGF α (squares), E40A (triangles) and Y13G (circles) for wild-type (A) and internalization impaired (B) EGFR

Total number of intracellular growth factor (closed symbols) is contrasted with the number of bound intracellular growth factor molecules (open symbols) and Eqn 11 (dashed lines) for each of the EGFR ligands. Simulations used the parameter values listed in Tables 1 and 2. The percentage of bound ligand is listed next to the corresponding internalization curves.

that extracellular binding is sufficiently fast to justify a steady-state approximation $C_s \approx R_{s0} L_o / (K_d + L_o)$ ($K_d \equiv k_f / k_t$) we can approximate the kinetics of intracellular complex as $dC_i/dt \approx k_f R_{s0} L_o / (K_d + L_o) - (k_x + k_{hr}) C_i$ with the solution:

$$\begin{aligned} C_i &\approx \frac{k_f R_{s0} L_o}{(k_x + k_{hr})(K_d + L_o)} [1 - e^{-(k_x + k_{hr})t}] \\ &= \frac{R_{i0} L_o}{(K_d + L_o)} [1 - e^{-(k_x + k_{hr})t}] \end{aligned} \quad (11)$$

Numerical simulations using baseline parameter estimates (Tables 1 and 2) illustrate that eqn (11) is a good approximation for all four ligands of EGFR (Figure 2B). We repeated the simulations depicted in Figure 2(B) for bolus concentrations in the range 0.1–100 nM and in each case also varied the endosomal volume between its reported minimal and maximal values, 4×10^{-15} and 2×10^{-13} litres [36] (Figure 3). More than 50% of the endosomal ligand is bound for all but three of the simulated cases. Moreover, more than 73% of the endosomal ligand is bound in simulations that assume minimal and basal endosomal volumes. Increasing the endosomal volume to its maximum resulted in a significant decrease in the percentage of bound ligand. For example, the percentage of bound TGF α and EGF decreased by $45.2 \pm 4.5\%$ and $24.4 \pm 11.0\%$ respectively as the endosomal volume was increased from its basal value to its maximum (S.D. reflects sensitivity to the initial bolus concentration). Simulations with

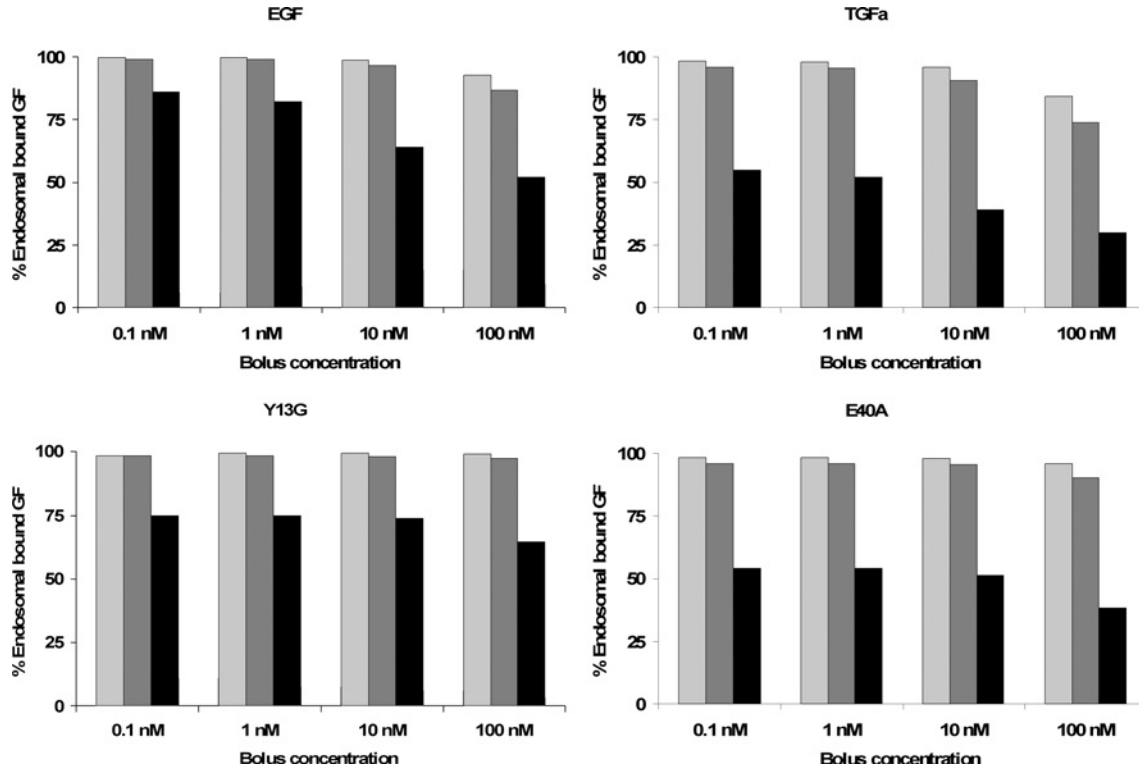


Figure 3 Percent bound endosomal ligand at the end of a 180 min incubation for a range of ligands, incubation concentrations and endosomal volumes of 4×10^{-15} litres/cell (light grey bars), 1×10^{-14} litres/cell (grey bars) and 2×10^{-13} litres/cell (black bars)

Simulation results are for internalization impaired receptors using the parameter estimates listed in Tables 1 and 2.

the basal endocytosis rate constant yielded essentially the same binding fractions, with deviations of the order of 1% from the results depicted in Figure 3. Interestingly, E40A ($45.0 \pm 4.8\%$) behaved like TGF α , whereas Y13G ($26.0 \pm 4.4\%$) behaved like EGF. These similarities will be explained by our analysis of eqns (1–6).

Taken together, the examples depicted in Figures 2 and 3 illustrate that the stability of endosomal complexes is not a simple function of their pI, and also depends nonlinearly on the magnitude of the endosomal volume and pre-incubation conditions. To gain a better understanding of these issues, we analysed eqns (1–6) for an accepted steady-state sorting protocol [7,36].

ANALYSIS OF STEADY-STATE SORTING

Steady-state sorting protocol

In the hypothetical experiments under consideration, following a 3h pre-incubation in warm binding medium (37°C), cells are washed in a cold mild-acid solution to remove the surface-bound ligand [6]. Subsequently, cell plates are transferred to a pre-warmed water bath (37°C) and incubated for various times before extracellular, surface and intracellular ligand concentrations are measured. The initial conditions corresponding to this protocol:

$$(L_o, C_s, C_i, L_i) = (0, 0, C_i^*, L_i^*) \quad (12)$$

uniquely define the initial number of free surface and intracellular receptors via eqn (10).

Model reduction

Typical *in vitro* cell densities justify a significant reduction of the model equations (see Supplementary Results at <http://www.BiochemJ.org/bj/402/bj4020537add.htm>). The total number of intracellular ligand molecules (eqn 9) is the sole dependent variable in the reduced model and its kinetics are governed by the first order differential equation:

$$dl_i/dt \approx -(k_x + k_{hr})C_-[l_i] - k_{hl}(l_i - C_-[l_i]) \quad (13)$$

with the initial condition:

$$l_i = l_i^*, t = 0 \quad (14)$$

Here:

$$k_1 \equiv k'_i/(N_A V e) \quad (15a)$$

$$K_M \equiv (k'_r + k_x + k_{hr})/k_1 \quad (15b)$$

and

$$C_-[l_i] \equiv \frac{(R_{i0} + K_M + l_i) - [(R_{i0} + K_M + l_i)^2 - 4R_{i0}l_i]^{1/2}}{2} \quad (16)$$

is the quasi-steady state number of endosomal receptor–ligand complexes. The concentrations of surface bound ligand and degraded ligand in the medium are both dependent variables in

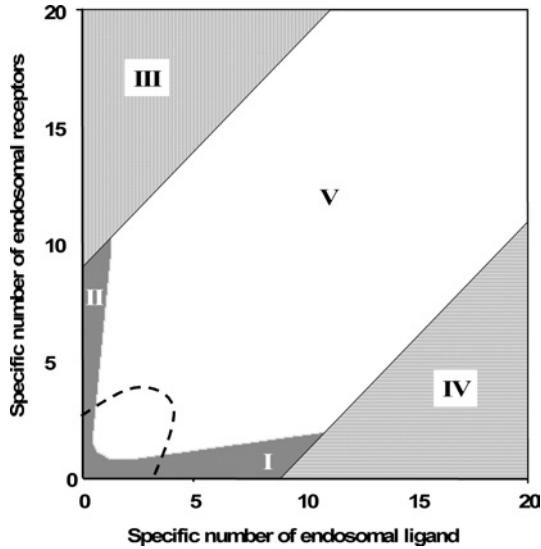


Figure 4 Classification of endosomal binding regimes as a function of the specific concentrations l_i^*/K_M and R_{i0}/K_M

Vertical lines, inequality 22 is valid, $C_e \approx l_i^*$; solid grey area, inequalities 20 or 21 are valid, $C_e \approx R_{i0}l_i^*/(K_M + R_{i0} + l_i^*)$; horizontal lines, inequality 23 is valid, $C_e \approx R_{i0}$; and, white area, the square root regime. Points lying beneath the diagonal imply that the total number of endosomal ligand molecules is larger than the total number of endosomal receptors, which is only possible with an unstable endosomal complex. Dashes enclose the region where the notion of a quasi-steady-state concentration of bound ligand may break down in the case of low endosomal desorption rate constant (see Supplementary Figure S1 at <http://www.BiochemJ.org/bj/402/bj4020537add.htm>). Importantly, the dashed region does not intersect the zone of stable binding (III).

the reduced model and are given, respectively, by:

$$C_s \approx k_x e^{-(k_r+k_t)t} \int_0^t C_i(s) e^{(k_r+k_t)s} ds \quad (17)$$

$$\approx k_x e^{-(k_r+k_t)t} \int_0^t C_-[l_i(s)] e^{(k_r+k_t)s} ds$$

and

$$dL_{deg}/dt \approx (n/N_A)\{k_{hr}C_-[l_i] + k_{hl}(l_i - C_-[l_i])\} \quad (18)$$

Stability of intracellular complex

The steady-state fraction of bound endosomal ligand $C_-[l_i^*]/l_i^*$ (eqn 16) is a direct measure of the stability of the endosomal complexes. Previous analysis shows that $C_-[l_i^*]/l_i^*$ decreases with total intracellular ligand as in any saturated binding state [30]. We now demonstrate that this fraction increases as R_{i0} rises relative to K_M and tends to unity as $R_{i0}/K_M \rightarrow \infty$ (see Supplementary Results). This implies that the necessary and sufficient condition for intracellular complex stability is:

$$R_{i0}/K_M \gg 1 \quad (19)$$

It is noteworthy that R_{i0}/K_M is inversely proportional to the endosomal volume, as this implies that endosomal complex stability decreases with increasing endosomal volume. Although the general expression for the fraction of bound endosomal ligand (eqn 16) is unintuitive, it reduces to intuitive forms in four partially overlapping but distinct zones of the plane of initial conditions (l_i^* , R_{i0}) (Figure 4). These zones are defined by the inequalities

[29,30]:

$$l_i^* + K_M \gg R_{i0}, \text{ zone I} \quad (20)$$

$$l_i^* \ll K_M + R_{i0}, \text{ zone II} \quad (21)$$

$$R_{i0} - l_i^* \gg K_M, \text{ zone III} \quad (22)$$

$$l_i^* - R_{i0} \gg K_M, \text{ zone IV} \quad (23)$$

and correspond to states of low-affinity binding ($C_i^*/l_i^* \ll 1$, zone I), linear binding ($C_i^*/l_i^* \approx R_{i0}/K_M$, zone II), high-affinity binding ($C_i^*/l_i^* \approx 1$, zone III) and binding under ligand excess ($C_i^*/l_i^* \approx R_{i0}/l_i^*$, zone IV) respectively. Numerical evaluation of $C_-[l_i^*]$ [30] illustrates that the stable endosomal-complex regime is fully spanned by the validity domain of inequality (eqn 22), and that the fraction of free endosomal ligand increases for total endosomal ligand levels that increasingly violate the inequality shown by eqn (23).

Apparent trafficking parameters

French and Lauffenburger [36] defined an apparent rate constant of intracellular ligand degradation, k_h , as the slope of the initial linear rise of the concentration of degraded ligand molecules in the medium, divided by the total concentration of intracellular ligand molecules, $(n/N_A)l_i^*$, eqn (18) implies:

$$k_h[l_i^*] \approx (k_{hr} - k_{hl})C_-[l_i^*]/l_i^* + k_{hl} \quad (24)$$

The decrease in $C_-[l_i^*]/l_i^*$ with l_i^* [30] implies that $k_h[l_i^*]$ increases (decreases) with total intracellular ligand (l_i^*) when $k_{hl} > k_{hr}$ ($k_{hl} < k_{hr}$) and that the maximal variation of $k_h[l_i^*]$ is bounded by the absolute difference between the degradation rate constants of free and bound ligand:

$$\max(k_h[l_i^*]) - \min(k_h[l_i^*]) \leq |k_{hl} - k_{hr}| \quad (25)$$

Moreover, the constraint $C_i \leq R_{i0}$ implies the high intracellular ligand load limit:

$$k_h[l_i^*] \approx k_{hl}, l_i^* \gg R_{i0} \quad (26)$$

Noting that endosomal ligand is depleted either by recycling or degradation, we can define an apparent intracellular clearance rate constant as:

$$t_f^{-1}[l_i^*] = k_h[l_i^*] + k_x C_-[l_i^*]/l_i^* = (k_x + k_{hr} - k_{hl})C_-[l_i^*]/l_i^* + k_{hl} \quad (27)$$

This notation reflects that t_f is the apparent time scale for endosomal ligand depletion. At high endosomal ligand loads clearance is dominated by degradation of free ligand.

$$t_f^{-1}[l_i^*] \approx k_{hl}, l_i^* \gg R_{i0} \quad (28)$$

French et al. [37] also defined an apparent recycling fraction, f_x , as the steady-state ratio of the recycling rate to the total clearance rate of endosomal ligand, $-dl_i/dt$. Using our results we find:

$$f_x[l_i^*] \equiv \frac{k_x C_-[l_i^*]}{(k_x + k_{hr})C_-[l_i^*] + k_{hl}(l_i^* - C_-[l_i^*])} \quad (29)$$

Table 3 Definition of lumped variables used in the evaluation of the uniformly valid approximations, Eqns (30–33)

Zone	$C_-[l_i^*]$	$k_h[l_i^*]$	t_i^{-1}
I	$\frac{R_{i0}l_i^*}{K_M + l_i^*}$	k_{hl}	$\frac{(k_x + k_{hr})R_{i0}}{K_M + l_i^*} + k_{hr}$
II	$\frac{R_{i0}l_i^*}{K_M + R_{i0}}$	$\frac{k_{hr}R_{i0} + k_{hl}K_M}{K_M + R_{i0}}$	$\frac{(k_x + k_{hr}R_{i0} + k_{hl}K_M)}{K_M + R_{i0}}$
III	l_i^*	k_{hr}	$k_x + k_{hr}$
IV,V	Eqn 16	Eqn 24	Eqn 27

The relationships:

$$f_x[l_i^*] \equiv \frac{k_x C_-[l_i^*]}{k_x C_-[l_i^*] + k_h[l_i^*]l_i^*} = \frac{1}{1 + k_h[l_i^*]/(C_-[l_i^*]/l_i^*)}$$

and

$$\frac{k_h[l_i^*]}{C_-[l_i^*]/l_i^*} = k_{hr} - k_{hl} + \frac{k_{hl}}{C_-[l_i^*]/l_i^*}$$

imply that $f_x[l_i^*]$, always decreases with total intracellular ligand.

Ligand time-course curves

The following approximate ligand time-course curves can be derived (see Supplementary Results) when either of inequalities 20–22 is valid:

$$l_i \approx l_i^* e^{-t/t_c} \quad (30)$$

$$L_0 \approx \frac{(n/N_A)k_r k_x C_-[l_i^*]}{k_r + k_t - t_i^{-1}} \left(\frac{1 - e^{-t/t_i}}{t_i^{-1}} - \frac{1 - e^{-(k_r+k_t)t}}{k_r + k_t} \right) \quad (31)$$

$$L_{deg} \approx (n/N_A)l_i^* k_h[l_i^*] t_i (1 - e^{-t/t_i}) \quad (32)$$

$$C_s \approx \frac{k_x C_-[l_i^*](e^{-t/t_i}) - e^{-(k_r+k_t)t}}{k_r + k_t - t_i^{-1}} \quad (33)$$

The parameters t_i , $C_-[l_i^*]$ and $k_h[l_i^*]$ are defined in Table 3. Double-exponential approximations have been used in the past to fit steady-state sorting data and can be derived directly from a base model that presumes the stability of internalized complexes [31]. That eqns (30–33) have the same functional form under conditions ranging from perfectly stable to fully dissociated endosomal complex suggests that their validity extends to states that violate inequalities 20–22 (Figure 4, zone V). To test this idea we shall also substitute the general forms of $C_-[l_i^*]$, $k_h[l_i^*]$ and $t_i[l_i^*]$ (eqns 16, 24 and 27) to evaluate eqns (30–33).

NUMERICAL EXAMPLES

Since the total number of endosomal ligand molecules after 3 h incubation (l_i^*) is an implicit function of the initial number of endosomal receptors (R_{i0}) there is no guarantee that inequalities (20–23) span all the physically relevant scenarios of endosomal complex stability. We used numerical examples to determine which zones of the (l_i^* , R_{i0}) plane are physically accessible and to test the approximations that lead to eqns (30–33).

Endosomal complex stability

To capture a range of potential steady-state sorting behaviours, we re-examined the relationship between the homeostatic internalized receptor number and endosomal ligand for the cases depicted in Figure 3. Remarkably, the reduced model (eqn 16) approximated the fraction of bound endosomal ligand for all 48 permutations depicted in Figure 3 to within a 1% error. Of these, over a quarter (13/48) are not classified in zones I–IV, over half (26/48) are classified as high-affinity binding states (zone III, Figure 4), seven as linear binding states (zone II, Figure 4) and two as states of ligand excess (zone IV, Figure 4). None of the cases are classified as states of low-affinity binding (zone I, Figure 4), suggesting that the number of intracellular receptors is not limiting for EGFR. Importantly, inequality 19 is satisfied by all four ligands at the basal endosomal volume, in agreement with their stability at low and basal endosomal volumes (Figure 3). At the highest reported endosomal volume, 2×10^{-13} litres/cell, we find that R_{i0}/K_M is 5.8 for EGF, 1.2 for TGF α , 1.2 for E40A and 2.9 for Y13G, consistent with their fractional binding at this volume (Figure 3).

These examples corroborate the validity of the suggested criterion for the stability of endosomal complexes (inequality 19). Since $K_M > (k_r/k_t)N_A V_e$, we can recast that criterion in terms of the endosomal dissociation constant, $K'_d \equiv k_r/k_t$. Namely, stability of the endosomal complex dictates that the concentration of endosomal receptors, $R_{i0}/(N_A V_e)$, be much higher than the endosomal dissociation constant:

$$R_{i0} \gg N_A V_e K'_d \quad (34)$$

Numerical simulations support this conclusion not only for mutant EGFR, but also for wild type EGFR (Figure 5).

Steady-state trafficking parameters

The validity of the reduced model for the cases considered in Figure 3 supports our definitions of steady state trafficking parameters (eqns 24, 27 and 29). At high endosomal ligand loadings $k_h[l_i^*]$ (Figures 6A and 6E), $t_i[l_i^*]$ (Figures 6B and 6F) and $f_x[l_i^*]$ (Figures 6C and 6G) depend strongly on the ratio k_{hl}/k_{hr} , whereas the fraction of bound endosomal ligand only varies with K_M and is therefore independent of k_{hl} (Figures 6D and 6H). The fraction of free endosomal ligand increases with endosomal ligand load and correspondingly $k_h[l_i^*]$ tends to the free ligand degradation rate constant. At endosomal ligand loads in excess of endosomal receptors the percentage of recycled ligand (Figures 6C and 6G) decreases, whereas the lifetime of endosomal ligand (Figures 6B and 6F) increases to its asymptotic value k_{hl}^{-1} .

It is noteworthy that the apparent trafficking parameter curves are all steeper for the lower endosomal volume (Figures 6A–D), and correspondingly lower K_M value. The shape of these curves reflects that $l_i \approx R_{i0}$ is the crossover point between high-affinity binding ($C_i^*/l_i^* \approx 1$; inequality 22) and binding under ligand excess ($C_i^*/l_i^* \approx R_{i0}/l_i^*$; inequality 23) and the width of the crossover is approximately $2 K_M$. In contrast, simulations that employ the maximal endosomal volume (Figures 6E–H) are representative of linear binding [$C_i^*/l_i^* \approx R_{i0}/(R_{i0} + K_M)$; inequality 21] at low intracellular ligand loads and the transition to excess ligand states (inequality 23) is smoother and occurs at higher ligand loads. Thus, at the basal endosomal volume the low ligand load limit of the apparent trafficking parameters is representative of the bound ligand, $k_h[l_i^*] \approx k_{hr}$, $t_i[l_i^*] \approx k_x + k_{hr}$ and $f_x[l_i^*] \approx 1/(1+k_{hr})$, whereas at maximal endosomal value the apparent trafficking parameters are also strongly influenced by the free ligand. These examples challenge the naïve perception that near-constant values of the steady state trafficking parameters

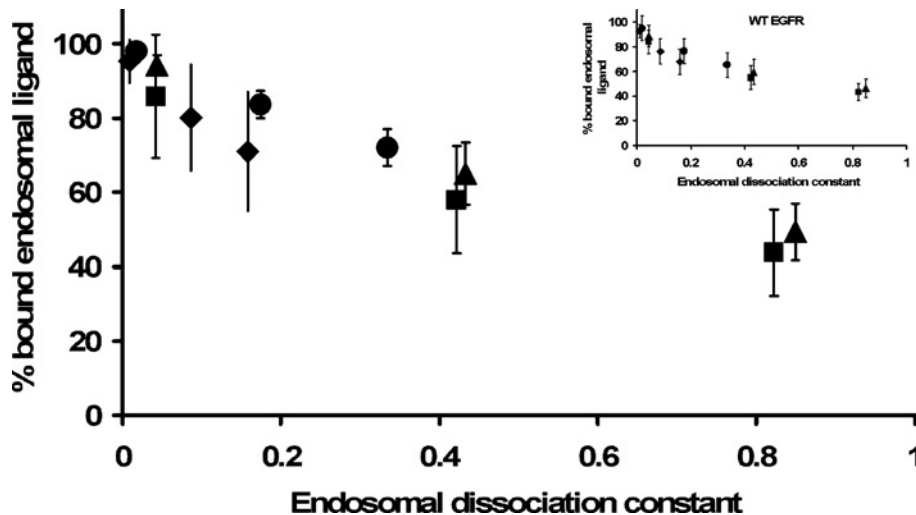


Figure 5 Endosomal binding versus endosomal dissociation constant

Simulations of the internalization protocol were used to evaluate the fraction of bound endosomal ligand at the end of 180 min incubation with extracellular EGF (◆), TGF α (■), E40A (▲), or Y13G (●). Results are averaged for pre-incubation concentrations of 0.1 nM, 1 nM, 10 nM and 100 nM, and plotted against a normalized dissociation constant $K'_d/R_{i0}N_A V_e$ for $V_e = 1 \times 10^{-14}$ litres, 1×10^{-13} litres and 2×10^{-13} litres. The inset panel shows the corresponding simulation results for downregulating receptors (k_e). Standard deviations reflect sensitivity to the magnitude of the pre-incubation concentration.

$k_{hi}[l_i^*]$, $k_x[l_i^*]$ and $f_x[l_i^*]$ are hallmarks of stable endosomal complexes.

Time-course curves

As experiments typically follow the time course of intact and degraded extracellular ligand and total intracellular ligand, we tested how well these quantities are estimated by their corresponding approximations (eqns 30–32) for a range of EGF and TGF α incubations. At basal endosomal volume, incubations with 0.1–10 nM EGF guarantee that $K_M/(R_{i0} + l_i^*) < 0.09$. Accordingly, the approximate forms corresponding to high-affinity binding (zone III, Table 3) closely approximate the initial time courses of the extracellular ligand and total intracellular ligand, and then begin to deviate after about 15 min, but match the overall trend in all cases (Figure 7, left-hand panels). Using the non-linear least squares regression error ($1 - R^2$) to estimate the *a posteriori* error, we find less than 9.2% error for the total endosomal EGF, less than 11.2% for the intact extracellular EGF and less than 24.7% for degraded EGF. The exceptionally high fractional *a posteriori* error for the degraded ligand is due to the differential degradation of ligand versus receptor (e.g., $k_{rl} = 4.5 k_{hr}$). For example, when $C_i = 0.90 l_i$, neglecting the term $k_{hi}(l_i - C_i/[i])$ in the equation for EGF degradation (eqn 18) leads to a 34% error in our approximate solution of this equation (eqn 32). Consequently, the error in degraded EGF decreases to less than 14% when the full-reduced model is used to evaluate eqns (30–32), whereas the errors in intact and total endosomal EGF are essentially unchanged. At basal endosomal volume, incubations with 0.1–10 nM TGF α (Figure 7, right-hand panels) display very similar trafficking kinetics to EGF (Figure 7, left-hand panels), in accord with the classification of these cases as states of high-affinity binding [$K_M/(R_{i0} + l_i^*) < 0.13$]. *A posteriori* we find less than 8.8% error for the total endosomal TGF α , less than 6.2% for the intact extracellular TGF α and less than 46.7% for degraded TGF α . The error in degraded TGF α decreases to less than 8.5% when using the full-reduced model to evaluate eqns (30–32), whereas the errors in intact and total endosomal TGF α are essentially unchanged.

Increasing the basal endosomal volume 20-fold to its maximum results in significantly more degraded EGF (1.6–2.1-fold) and TGF α (3.2–3.7-fold), but only slightly more intact extracellular (Figures 8A and 8D) and endosomal (Figures 8C and 8F) EGF and TGF α . These trends are captured by the reduced model, which observably deviates from the numerical time-course curves only after approx. 15 min. Interestingly, whereas approximately the same percentage (4%) of preloaded EGF (Figure 7B) and TGF α (Figure 7E) were degraded at basal endosomal volume, at maximal endosomal volume a significantly smaller percentage of preloaded EGF (6.7–9.1%, Figure 8B) is degraded than preloaded TGF α (14.6–18.2%, Figure 8E). This heightened sensitivity of total ligand degradation to the magnitude of the endosomal volume stems from the differential degradation of free and bound endosomal ligand (e.g., $k_{hi} \gg k_{hr}$). For example, in zone III, where the majority of preloaded ligand is in complex, the fractional change in total recycled ligand and total degraded ligand upon dissociation of x endosomal complexes is $-x/l_i$ and $(k_{hi}/k_{hr})x/l_i$ respectively.

DISCUSSION

EGF and TGF α both bind EGFR, but, whereas EGF remains predominantly bound to EGFR inside the sorting endosome, a significant fraction of endosomal TGF α is thought to be dissociated [4,5,8]. Yet, our numerical simulations using published parameter estimates (Tables 1 and 2) surprisingly predict that internalized TGF α is predominantly bound to EGFR, and to an extent similar to EGF (Figure 2). This discrepancy can be understood in the major part when one considers endosomal volume as a critical parameter in growth factor–receptor association. TGF α and EGF follow similar binding kinetics. Both are bound to the receptor when simulations consider low endosomal volumes and are dissociated as the volume values are increased (Figure 3). Full appreciation of the relevance of predicted binding scenarios, however, requires introduction of a means of prioritizing the volume estimation. The wide range of published volume estimates can then be appreciated if these values are scaled to other cellular kinetic parameters.

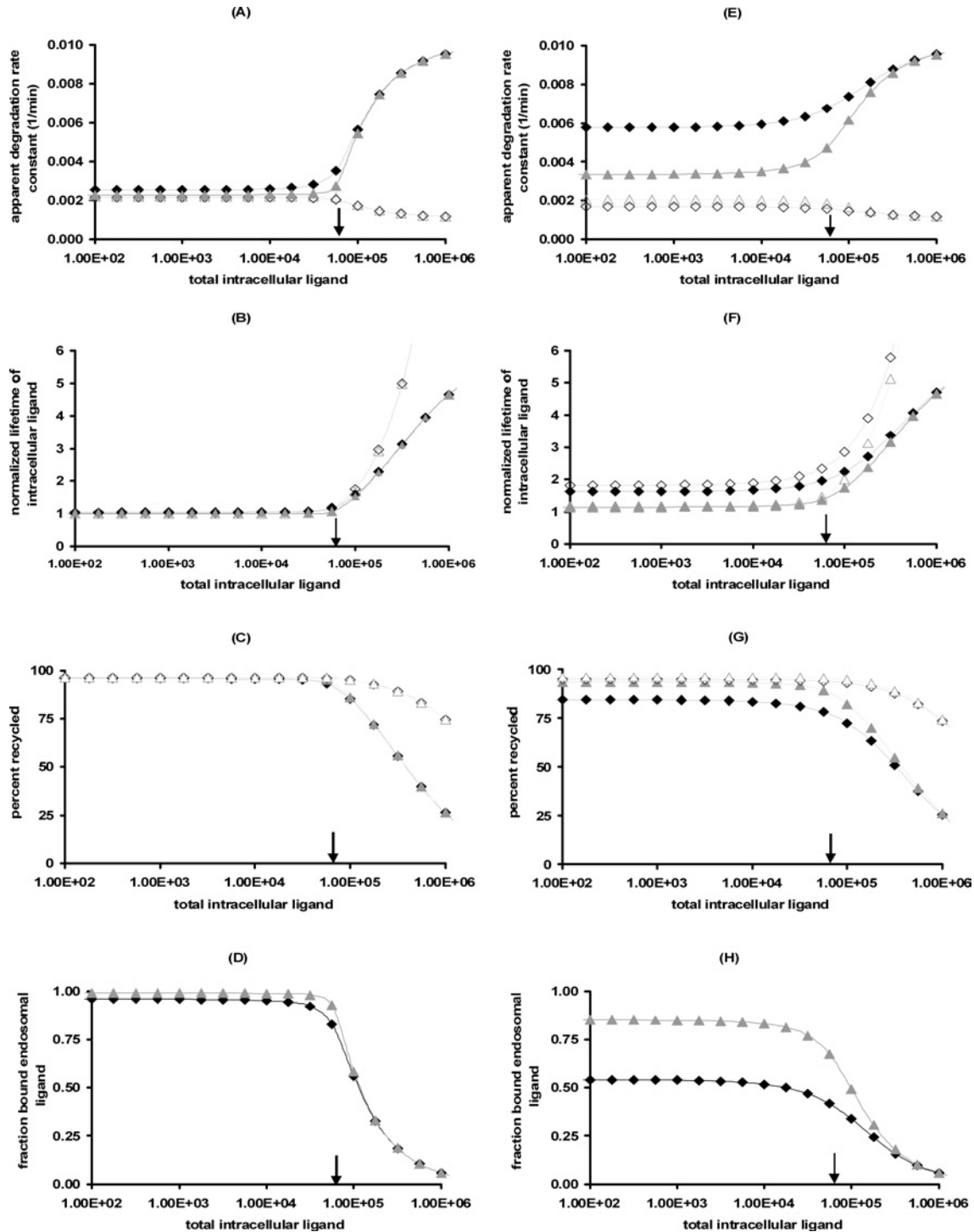


Figure 6 Apparent trafficking constants as a function of the endosomal volume

Left-hand panels, $V_e = 1 \times 10^{-14}$ litres/cell; right-hand panels, $V_e = 2 \times 10^{-13}$ litres/cell. (A and E) $k_n[I_r]$, (B and F) $(k_x + k_{tr})t_i[I_r]$, (C and G) $100f_x[I_r]$ and (D and H) $C.[I_r]/I_r$. Eqns (24, 27 and 29) are evaluated for EGF (triangles) and TGF α (diamonds) with $k_{ni} = 0.001 \text{ min}^{-1}$ (closed symbols) or $k_{ni} = 0.0011 \text{ min}^{-1}$ (open symbols). $k_{ni} - k_{tr}$ is positive for the closed symbols and negative for the open symbols, but K_M is unaltered by variations in k_{ni} . Solid arrows denote the location of the threshold value $l_i = R_{10}$.

A central result of the present analysis is that the fraction of bound endosomal ligand is governed by a single dimensionless parameter (inequality 19) that depends on three primary factors: the total endosomal volume, the apparent endosomal dissociation constant and the number of endosomal receptors.

Though standard protocols have shed great light on receptor kinetics, they are not sensitive to the binding state of the internalized ligand. A mathematical manifestation of such insensitivity to the binding state of internalized ligand is that ligand kinetics are approximated by the same formulae (eqns 30–33)

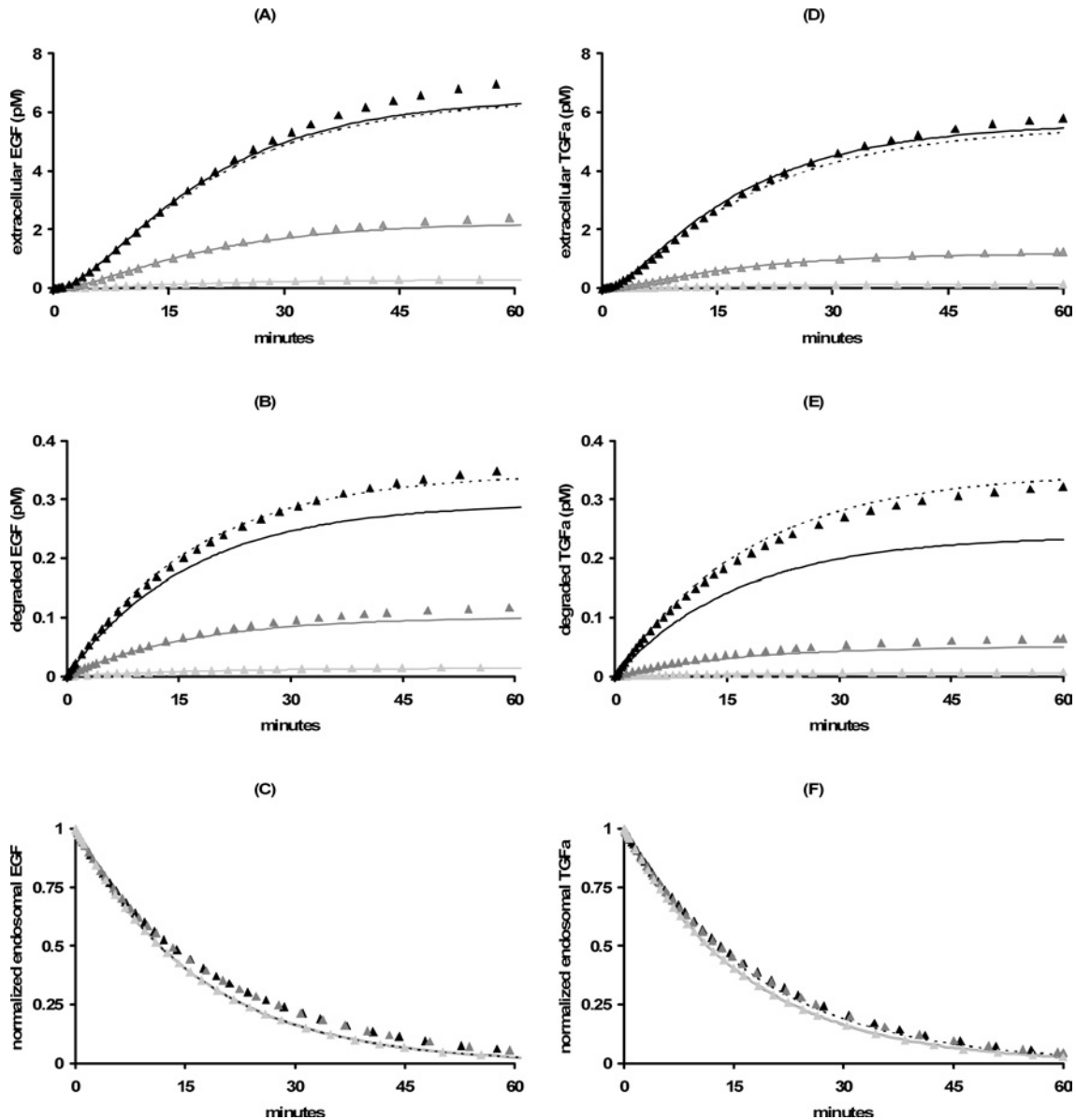


Figure 7 Trafficking kinetics at basal endosomal volume

Eqns (30–32) specialized for the square root regime (dashed lines; zone V) or the high affinity binding limit (solid lines; zone III; Table 3) are contrasted with the corresponding simulations of the full model for a range of (180 min) pre-incubation concentrations of labelled EGF (left-hand panels) or TGF α (right-hand panels): 0.1 nM (light grey triangles), 1.0 nM (grey triangles) and 10 nM (black triangles). Parameter values are as listed in Tables 1 and 2. **(A and D)** Intact extracellular ligand, **(B and E)** degraded extracellular ligand and **(C and F)** total endosomal ligand.

for states that encompass the limits of perfectly stable ($C_i \approx l_i$) and irreversibly dissociating ($C_i \ll l_i$) endosomal complex. In this sense, our analysis illustrates that the study of growth factor trafficking may be hampered by issues of kinetic distinguishability [38]. Nevertheless, the stability of the internalized complex can be resolved by determining the pools of free and bound endosomal ligand. The fraction of bound ligand can be determined indirectly from plots of the apparent trafficking parameters versus intracellular ligand load (Figure 6). In particular, the difference between the apparent clearance rate constant $t_i^{-1}[l_i^*]$ (eqn 27) and the apparent degradation rate $k_h[l_i^*]$ (eqn 24) is proportional to the fraction of bound ligand, $C_i[l_i^*]/l_i^*$ and is thus a direct measure of complex stability. As $C_i[l_i^*]/l_i^*$ is near-constant only when the total number of endosomal ligand molecules is smaller than the apparent endosomal dissociation constant, K_M (Figures 6D

and 6H), the latter can be estimated as the intracellular ligand loading for which $t_i^{-1}[l_i^*] - k_h[l_i^*]$ drops to half its value.

Endosomal volume

The impact of endosomal volume can be profound. Dissociation of the receptor–ligand complex is predicted to be enhanced with increasing endosomal volume (Figure 3 and inequality 34). The dependence of binding on volume has been noted in a computational study of a more detailed model of endosomal sorting [36], but has never been prioritized before. Our results illustrate the importance of directly estimating the endosomal volume for a given cell type and of reporting a sensitivity analysis on this parameter. Schoeberl et al. [25] set the endosomal volume at 0.00003% of the intracellular volume (4.2×10^{-18} litres),

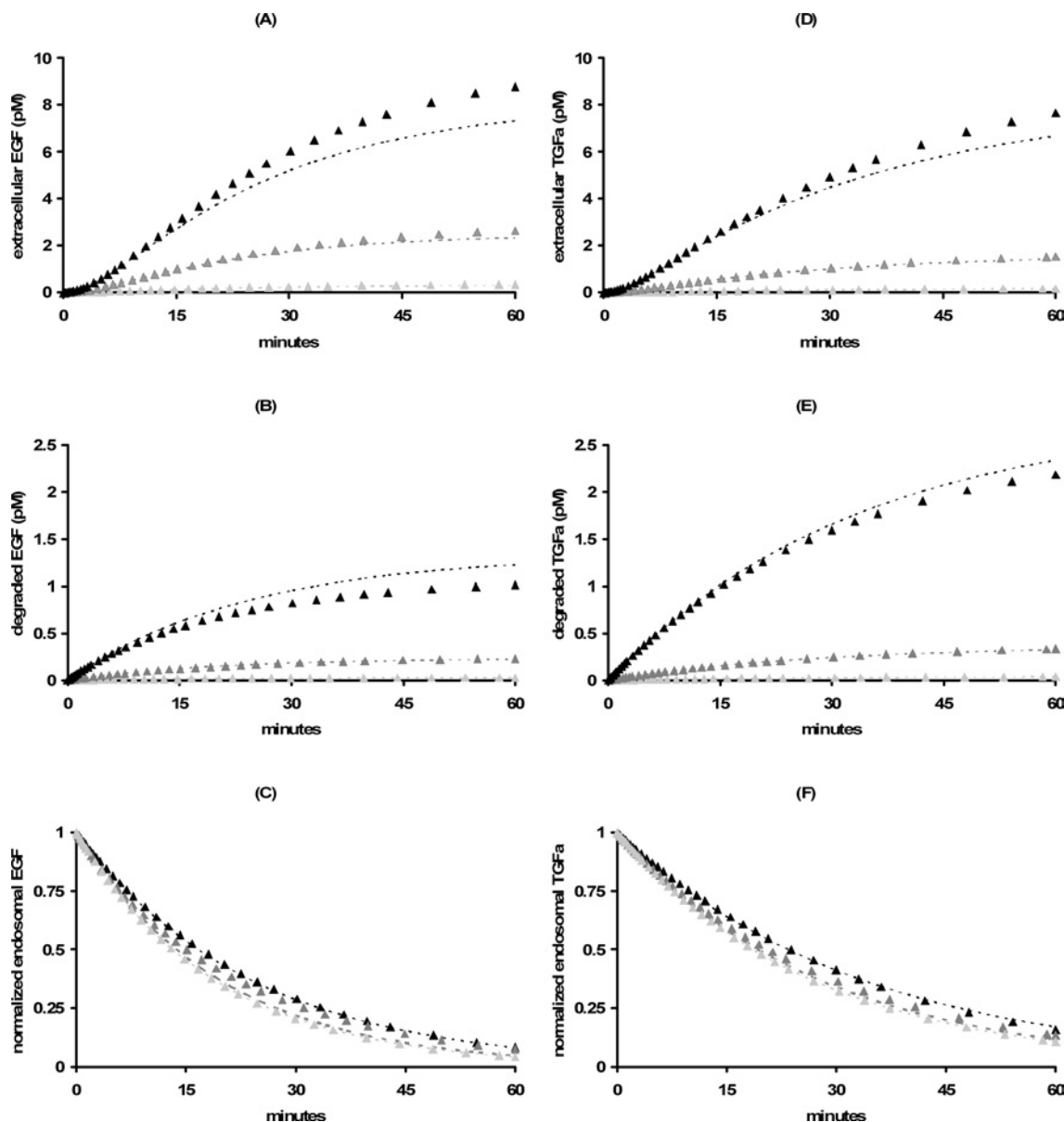


Figure 8 Trafficking kinetics at maximal endosomal volume

Dashed lines, eqns (30–32) specialized for the square root regime (zone V; Table 3) are contrasted with the corresponding simulations of the full model for a range of (180 min) pre-incubation concentrations of labelled EGF (left-hand panels) or TGF α (right-hand panels): 0.1 nM (light grey triangles), 1.0 nM (grey triangles) and 10 nM (black triangles). Parameter values are as in Tables 1 and 2, except for the endosomal volume, which is set at 2×10^{-13} litres/cell. (**A** and **D**) Intact extracellular ligand, (**B** and **E**) degraded extracellular ligand and (**C** and **F**) total endosomal ligand.

whereas others [39] set it to 100 % of the total intracellular volume (1.0×10^{-12} litres). Yet volume estimates predetermine the fate of the endosomal ligand, almost irrespective of the binding constants (Figure 3). Simulations that employ the smaller value invariably result in a very stable endosomal complex, whereas simulations that employ larger volumes invariably create especially unstable complexes.

Endosomal dissociation constant

In our model, endosomal volume and the number of intracellular receptors at homeostasis are intrinsic cell parameters and do not vary with ligand type. Thus, for a given cell line, the endosomal ligand–receptor dissociation constant determines the differential stability of intracellular signalling complexes of various ligands of

the same receptor. For example, the range of reported equilibrium dissociation constants (Table 2) dictates that the stability of E40A should be similar to that of TGF α , whereas the stability of Y13G should be similar to EGF over a wide range of pre-incubation conditions and endosomal volumes (Figure 3).

The finding that the criteria for endosomal stability of constitutively trafficking receptors (inequalities 19 and 34) do not depend on the receptor internalization rate constant, strongly suggests that these criteria remain valid for down-regulating receptors. Numerical simulations support this conclusion (Figure 5) and reflect that down-regulation increases the total number of endosomal receptors beyond their initial number, R_{10} , such that, if inequality 19 is valid at time zero, it remains so when $R_{1,\text{tot}} \equiv R_i + C_i$ is substituted for R_{10} . Moreover, numerical simulations of internalization experiments corresponding to wild-type

down-regulating receptors, illustrate that the fraction of bound intracellular ligand is well approximated by the relationship

$$C_{\text{[L]}} \equiv \left\{ (R_{\text{i,tot}} + K_{\text{M}} + l_{\text{i}}) - [(R_{\text{i,tot}} + K_{\text{M}} + l_{\text{i}})^2 - 4R_{\text{i,tot}}l_{\text{i}}]^{1/2} \right\} / 2l_{\text{i}}$$

The significance of our analysis is not limited to EGFR. For example, inequality 34 provides a rational basis for the empiric finding that the recycling fraction of IL-2 increases with endosomal dissociation constant [33], once allowance is made for the fact that in this system free ligand is recycled rather than being bound, as is the case in EGFR trafficking.

Receptor expression

Stability of endosomal signalling complexes is not only a property of the specific ligand-receptor pair, but also depends upon the intracellular milieu. The stability of the endosomal receptor complex is then a 'systems property' of the cell that is amenable to evolutionary optimization and dynamic control. Cells can modulate the level of endosomal signalling by varying their endosomal volume, and by regulating one receptor over another (inequality 34). At homeostasis, the number of endosomal receptors is determined by the balance of receptor synthesis and degradation (eqn 8). Thus, it becomes possible to stabilize an otherwise unstable receptor complex by increasing the rate constant of receptor synthesis (inequality 34). For example, at the maximal endosomal volume, the fraction of bound endosomal TGF α at the end of a 180 min incubation with 10 nM TGF α increases from 39% at $k_{\text{syn}} = 130$ receptors/cell \cdot min $^{-1}$ to 83% at $k_{\text{syn}} = 1300$ receptors/cell \cdot min $^{-1}$ ($R_{\text{s0}} = 1185760$ and $R_{\text{i0}} = 590910$). The corresponding numbers for wild-type EGFR are 39% and 77%. In a sense then, the convenience of conducting experiments with cell lines that overexpress receptors, might create a biased state where endosomal complexes are artificially stable. The finding that complex stability increases with the number of endosomal receptors also cautions against the practice of neglecting the internalization flux of unoccupied receptors in computational studies of receptor sorting [36]. Numerical simulations illustrate that such neglect significantly misrepresents the dynamics of endosomal sorting as well as its steady-state (see Supplementary Results at <http://BiochemJ.org/bj/402/bj4020537add.htm>).

At the maximal endosomal volume $R_{\text{i0}} > K_{\text{M}}$ for all four EGFR agonists (Tables 1 and 2), implying that all four agonists are relatively stable after internalization. It is instructive to compare these findings with other cytokines and cells that express several hundred intracellular receptors two orders of magnitude less than EGFR in B82 fibroblasts. As an example, $R_{\text{i0}} > 7K_{\text{M}}$ for IL-2 and its analogue 2D1 even at the maximal endosomal volume [33], implying that both cytokines remain predominantly bound to their endosomal receptors. Thus, the experimental estimates of the equilibrium dissociation constant of 2D1 and IL-2 at pH 6.0 cannot explain why the steady-state recycling fraction of 2D1 is 1.7-fold less than that of IL-2 in these cells [33]. This example raises the question of whether extracellular binding constants measured at pH 6.0 are representative of endosomal binding?

Surface signalling versus endosomal signalling

It is now appreciated that growth factor receptors can remain phosphorylated in the sorting endosome and can continue to signal from this environment. Endosomal signalling is biologically significant, and is capable of independently suppressing apoptosis [40] and inducing proliferation [41]. Compartmentalization of signalling molecules suggests a differential role for surface and endosomal signalling [17–19]. Thus, the absolute numbers of surface and intracellular signalling complexes, as well as their

ratios are important factors that determine cellular responses and distinguish between extracellular cues. The total number of signalling complexes is limited by the total number of receptors and the magnitude and kinetics of the extracellular ligand perturbation. Our analysis sheds new light on the factors governing the ratio of surface and intracellular signalling complexes. For stable intracellular complexes the ratio of internalized to surface complexes is independent of ligand, and is determined by the balance of endocytosis, degradation and recycling $C_{\text{i}}/C_{\text{s}} \approx k_{\text{e}}/(k_{\text{hr}} + k_{\text{x}})$ (eqn 4 and [42]). Intracellular dissociation alters this simple relationship and allows greater control over the signalling bias. The number of stable internalized complexes should increase with the ratio $V_{\text{e}}^{-1}R_{\text{i0}}/(N_{\text{A}}K'_{\text{d}})$ (inequality 34). Similarly, the number of surface complexes should increase with the ratio $nR_{\text{s0}}/[N_{\text{A}}K_{\text{d}}(\text{app})]$ where $K_{\text{d}}(\text{app}) = (k_{\text{r}}/k_{\text{e}})(k_{\text{r}} + k_{\text{e}})/k_{\text{f}}$ [22] for down-regulating receptors and $K_{\text{d}}(\text{app}) = (k_{\text{r}} + k_{\text{i}})/k_{\text{f}}$ for constitutively trafficking receptors (eqn 11). Thus, different biases between surface and internalized receptor complex are expected. Cell density, endosomal volume, surface and intracellular receptor levels at homeostasis, and the ratio of the dissociation constant of the surface complex to the endosomal complexes (Table 2) will all influence this bias. As the kinetics of growth factor presentation to surface receptors can have an impact on the stability of internalized complexes, delivery modalities might be designed to minimize or maximize endosomal signalling to meet specific pharmacologic goals. It may well be that this is the manner by which endogenous cytokines mediate growth factor signalling bias. Up-regulation of EGFR by TGF α [43], VEGF (vascular endothelial growth factor) [44] and PDGF (platelet-derived growth factor) [45] (but not EGF), or up-regulation of the PDGF receptors by FGF2 (fibroblast growth factor 2) [46] may fall into this category. Our results suggest that cytokine-induced upregulation not only amplifies surface signalling, but also pushes the signalling bias towards intracellular signals as both the number of intracellular receptors and the proportion of bound receptors increases.

Limitations

The generic model studied in the present paper is based on three simplifying assumptions: (a) that the recycling rate constant of endosomal receptors is independent of occupancy; (b) that sorting to the lysosome is nonspecific; and (c) that fluid phase uptake is negligible. Assumption (a) is valid for a class of EGFR including the kinase-active internalization impaired receptor c'973 [26], but is invalid for a range of wild-type and internalization impaired EGFRs [47]. However, as our analysis illustrates, intracellular dissociation alters the apparent recycling rate constant of occupied receptors, whereas the recycling rate constant of unoccupied receptors is set by homeostasis (eqn 8). Assumption (b) is valid for ligands that are predominantly in fluid phase inside endosomes (presumably TGF α). Experiments suggest that lysosomal sorting can saturate at higher intracellular loads of EGF [37,47]. Although specific lysosomal sorting is beyond the scope of our model, we expect the criterion for complex stability (inequality 34) to remain valid under more general circumstances. This may be the case as this inequality reflects a thermodynamic balance of receptor concentration and the equilibrium dissociation constant. Thus, at sufficiently low endosomal volumes, EGF and TGF α are predicted to be predominantly bound to EGFR, and we would expect both to saturate the lysosomal sorting machinery. At the extreme of high endosomal volume we would anticipate both EGF and TGF α to be predominantly in fluid phase.

Internalization of molecules by fluid-phase endocytosis is proportional to their concentration in the extracellular fluid, and

can be accounted for in our model by adding the ligand depletion term $k_{ip}N_A L_0$ in eqn (3), where k_{ip} has the dimensions of volume \cdot cell $^{-1} \cdot$ min $^{-1}$ [23]. The contribution of fluid-phase internalization relative to receptor mediated internalization scales as the dimensionless ratio $k_{ip}N_A L_0/(k_c C_s)$. Estimating the rate of receptor internalization as $k_c C_s \approx k_c R_{s0} L_0/(K_d + L_0)$ we conclude that fluid-phase uptake is significant when $k_{ip}N_A(K_d + L_0)/k_c R_{s0} > 0.1$. The reported value for NR6 fibroblasts of $k_{ip} \leq 3.4 \times 10^{-16}$ litres \cdot cell $^{-1} \cdot$ min $^{-1}$ [48] suggests that in these cells fluid uptake only becomes significant for extremely high extracellular ligand concentrations ($L_0 > 60K_d = 150$ nM). Thus, assumption (c) seems to be justified for the examples considered here. At high extracellular ligand concentrations that render fluid-phase uptake significant, the steady state number of intracellular ligand molecules can significantly exceed the number of intracellular receptors. In such cases the fraction of bound endosomal ligand no longer reflects the stability of the internalized ligand–receptor complexes. Although the detailed analysis of the effects of fluid-phase ligand uptake are beyond the scope of this work, first principles considerations (e.g., Le Chatelier's principle) imply that fluid-phase internalization would tend to stabilize the endosomal ligand–receptor complex, thereby enhancing intracellular signalling. Moreover, when fluid-phase internalization dominates, the majority of ligand molecules enter the cell unbound, rather than receptor bound as assumed in our model, and endosomal complex stability is rendered independent of endosomal volume.

Conclusions

Mathematical modelling of biological systems is indispensable, particularly when experimental studies define areas of importance, but cannot characterize them fully. Numerical simulations of model equations can generate a wide spectrum of possible scenarios *in silico*, but are inefficient at prioritizing critical determinants. Augmentation of numerical simulation by careful time-scale analysis can provide direct information on parameter sensitivity over a wide range of values. This numerical–analytical approach has provided a novel insight into the predominant factors that govern the average lifetime of intracellular signalling growth factor complexes. Such insights call for a reconsideration of the conventional view that growth factor–receptor complex stability is solely governed by endosomal pH.

This work was supported in part by grants from the National Institutes of Health to E. R. E. (R01 HL 49039 and HL 67246) and a Philip Morris External Research Postdoctoral Fellowship to A. R. T. We thank Professor M. Nugent and Dr D. Wu for careful reading of the manuscript and useful suggestions.

REFERENCES

- Mukherjee, S., Ghosh, R. N. and Maxfield, F. R. (1997) Endocytosis. *Physiol. Rev.* **77**, 759–803
- Maxfield, F. R., Schlessinger, J., Shechter, Y., Pastan, I. and Willingham, M. C. (1978) Collection of insulin, EGF and alpha2-macroglobulin in the same patches on the surface of cultured fibroblasts and common internalization. *Cell* **14**, 805–810
- Ciechanover, A., Schwartz, A. L., Dautry-Varsat, A. and Lodish, H. F. (1983) Kinetics of internalization and recycling of transferrin and the transferrin receptor in a human hepatoma cell line. Effect of lysosomotropic agents. *J. Biol. Chem.* **258**, 9681–9689
- Sorkin, A. D., Teslenko, L. V. and Nikolsky, N. N. (1988) The endocytosis of epidermal growth factor in A431 cells: a pH of microenvironment and the dynamics of receptor complex dissociation. *Exp. Cell Res.* **175**, 192–205
- Sorkin, A., Kornilova, E., Teslenko, L., Sorkin, A. and Nikolsky, N. (1989) Recycling of epidermal growth factor–receptor complexes in A431 cells. *Biochim. Biophys. Acta.* **1011**, 88–96
- Korc, M. and Finman, J. E. (1989) Attenuated processing of epidermal growth factor in the face of marked degradation of transforming growth factor-alpha. *J. Biol. Chem.* **264**, 14990–14999
- Ebner, R. and Derynck, R. (1991) Epidermal growth factor and transforming growth factor-alpha: differential intracellular routing and processing of ligand–receptor complexes. *Cell Regul.* **2**, 599–612
- Haugh, J. M., Schooler, K., Wells, A., Wiley, H. S. and Lauffenburger, D. A. (1999) Effect of epidermal growth factor receptor internalization on regulation of the phospholipase C- γ 1 signaling pathway. *J. Biol. Chem.* **274**, 8958–8965
- Di Guglielmo, G. M., Baass, P. C., Ou, W. J., Posner, B. J. and Bergeron, J. J. (1994) Compartmentalization of SHC, GRB2 and mSOS, and hyperphosphorylation of Raf-1 by EGF but not insulin in liver parenchyma. *EMBO J.* **13**, 4269–4277
- Haugh, J. M., Huang, A. C., Wiley, H. S., Wells, A. and Lauffenburger, D. A. (1999) Internalized epidermal growth factor receptors participate in the activation of p21(ras) in fibroblasts. *J. Biol. Chem.* **274**, 34350–34360
- Wang, Y., Pennock, S. D., Chen, X., Kazlauskas, A. and Wang, Z. (2004) Platelet-derived growth factor receptor-mediated signal transduction from endosomes. *J. Biol. Chem.* **279**, 8038–8046
- Bevan, A. P., Krook, A., Tikerpaee, J., Seabright, P. J., Siddle, K. and Smith, G. D. (1997) Chloroquine extends the lifetime of the activated insulin receptor complex in endosomes. *J. Biol. Chem.* **272**, 26833–26840
- Lampugnani, M. G., Orsenigo, F., Gagliani, M. C., Tacchetti, C. and Dejana, E. (2006) Vascular endothelial cadherin controls VEGFR-2 internalization and signaling from intracellular compartments. *Cell Biol.* **174**, 593–604
- Grimes, M. L., Zhou, J., Beattie, E., Yuen, E., Hall, D., Valletta, J., Topp, K., LaVail, J., Bunnett, N. and Mobley, W. C. (1996) Endocytosis of activated TrkA: evidence that nerve growth factor induces formation of signaling endosomes. *J. Neurosci.* **16**, 7950–7964
- Waterman, H., Sabanai, I., Geiger, B. and Yarden, Y. (1998) Alternative intracellular routing of ErbB receptors may determine signaling potency. *J. Biol. Chem.* **273**, 13819–13827
- Ouyang, X., Gulliford, T., Huang, G. and Epstein, R. J. (1999) Transforming growth factor-alpha short-circuits downregulation of the epidermal growth factor receptor. *J. Cell Physiol.* **179**, 52–57
- Wakshull, E. M. and Wharton, W. (1985) Stabilized complexes of epidermal growth factor and its receptor on the cell surface stimulate RNA synthesis but not mitogenesis. *Proc. Natl. Acad. Sci. USA.* **82**, 8513–8517
- Haugh, J. M. and Lauffenburger, D. A. (1997) Physical modulation of intracellular signaling processes by locational regulation. *Biophys. J.* **72**, 2014–2031
- Ceresa, B. P., Kao, A. W., Santeler, S. R. and Pessin, J. E. (1998) Inhibition of clathrin-mediated endocytosis selectively attenuates specific insulin receptor signal transduction pathways. *Mol. Cell Biol.* **18**, 3862–3870
- Kholodenko, B. N. (2003) Four-dimensional organization of protein kinase signaling cascades: the roles of diffusion, endocytosis and molecular motors. *J. Exp. Biol.* **206**, 2073–2082
- Knauer, D. J., Wiley, H. S. and Cunningham, D. D. (1984) Relationship between epidermal growth factor receptor occupancy and mitogenic response. Quantitative analysis using a steady state model system. *J. Biol. Chem.* **259**, 5623–5631
- Wiley, S. H. and Cunningham, D. D. (1981) A steady state model for analyzing the cellular binding, internalization and degradation of polypeptide ligands. *Cell* **25**, 433–440
- Lauffenburger, D. A. and Linderman, J. J. (1993) *Receptors: Models for Binding, Trafficking and Signaling*. Oxford University Press, New York (Chapter 3)
- Brightman, F. A. and Fell, D. A. (2000) Differential feedback regulation of the MAPK cascade underlies the quantitative differences in EGF and NGF signalling in PC12 cells. *FEBS Lett.* **482**, 169–174
- Schoeberl, B., Eichler-Jonsson, C., Gilles, E. D. and Muller, G. (2002) Computational modeling of the dynamics of the MAP kinase cascade activated by surface and internalized EGF receptors. *Nat. Biotechnol.* **20**, 370–375
- Starbuck, C. and Lauffenburger, D. A. (1992) Mathematical model for the effects of epidermal growth factor receptor trafficking dynamics on fibroblast proliferation responses. *Biotechnol. Prog.* **2**, 132–143
- Chen, W., Lazar, C., Lund, K., Welsh, J., Chang, C., Walton, G., Der, C., Wiley, H. S., Gill, G. N. and Rosenfeld, M. G. (1989) Functional independence of the epidermal growth factor receptor from a domain required for ligand-induced internalization and calcium regulation. *Cell* **59**, 33–43
- Baulida, J., Krauss, M. H., Alimandi, M., Di Fiore, P. P. and Carpenter, G. (1996) All ErbB receptors other than the epidermal growth factor receptor are endocytosis impaired. *J. Biol. Chem.* **271**, 5251–5257
- Tzafirri, A. R. (2003) Michaelis–Menten kinetics at high enzyme concentrations. *Bull. Math. Biol.* **65**, 1111–1129
- Tzafirri, A. R. and Edelman, E. R. (2007) Quasi-steady state kinetics at enzyme and substrate concentrations in excess of the Michaelis–Menten constant. *J. Theor. Biol.*, doi:10.1016/j.jtbi.2006.12.005

- 31 Tzafiriri, A. R., Wu, D. and Edelman, E. R. (2004) Analysis of compartmental models of ligand-induced endocytosis. *J. Theor. Biol.* **229**, 127–138
- 32 Schwartz, A. L., Fridovich, S. E. and Lodish, H. F. (1982) Kinetics of internalization and recycling of the asialoglycoprotein receptor in a hepatoma cell line. *J. Biol. Chem.* **257**, 4230–4237
- 33 Fallon, E. M. and Lauffenburger, D. A. (2000) Computational model for effects of ligand/receptor binding properties on interleukin-2 trafficking dynamics and T cell proliferation response. *Biotechnol. Prog.* **16**, 905–916
- 34 Sarkar, C. A. and Lauffenburger, D. A. (2003) Cell-level pharmacokinetic model of granulocyte colony-stimulating factor: implications for ligand lifetime and potency *in vivo*. *Mol. Pharmacol.* **63**, 147–158
- 35 French, A. R., Tadaki, D. K., Niyogi, S. K. and Lauffenburger, D. A. (1995) Intracellular trafficking of epidermal growth factor family ligands is directly influenced by the pH sensitivity of the receptor/ligand interaction. *J. Biol. Chem.* **270**, 4334–4340
- 36 French, A. R. and Lauffenburger, D. A. (1997) Controlling receptor/ligand trafficking: effects of cellular and molecular properties on endosomal sorting. *Ann. Biomed. Eng.* **25**, 690–707
- 37 French, A. R., Sudlow, G. P., Wiley, H. S. and Lauffenburger, D. A. (1994) Postendocytotic trafficking of epidermal growth factor-receptor complexes is mediated through saturable and specific endosomal interactions. *J. Biol. Chem.* **269**, 15749–15755
- 38 Erdi, P. and Toth, J. (1989) *Mathematical Models of Chemical Reactions: Theory and Applications of Deterministic and Stochastic Models*. Princeton University Press, Princeton, NJ
- 39 Athale, C., Mansury, Y. and Deisboeck, T. S. (2005) Simulating the impact of a molecular 'decision-process' on cellular phenotype and multicellular patterns in brain tumors. *J. Theor. Biol.* **233**, 469–481
- 40 Wang, Y., Pennock, S., Chen, X. and Wang, Z. (2002) Endosomal signaling of epidermal growth factor receptor stimulates signal transduction pathways leading to cell survival. *Mol. Cell Biol.* **22**, 7279–7290
- 41 Pennock, S. and Wang, Z. (2003) Stimulation of cell proliferation by endosomal epidermal growth factor receptor as revealed through two distinct phases of signaling. *Mol. Cell Biol.* **23**, 5803–5815
- 42 Wiley, H. S., Herbst, J. J., Walsh, B. J., Lauffenburger, D. A., Rosenfeld, M. G. and Gill, G. N. (1991) The role of tyrosine kinase activity in endocytosis, compartmentation, and down-regulation of the epidermal growth factor receptor. *J. Biol. Chem.* **266**, 11083–94
- 43 Reddy, C. C., Niyogi, S. K., Wells, A., Wiley, H. S. and Lauffenburger, D. A. (1996) Engineering epidermal growth factor for enhanced mitogenic potency. *Nat. Biotechnol.* **14**, 1696–1699
- 44 Mathur, R. S. and Mathur, S. P. (2005) Vascular endothelial growth factor (VEGF) up-regulates epidermal growth factor receptor (EGF-R) in cervical cancer *in vitro*: this action is mediated through HPV-E6 in HPV-positive cancers. *Gynecol. Oncol.* **97**, 206–213
- 45 Heldin, C. H., Wasteson, A. and Westermark, B. (1982) Interaction of platelet-derived growth factor with its fibroblast receptor. Demonstration of ligand degradation and receptor modulation. *J. Biol. Chem.* **257**, 4216–4221
- 46 Schollmann, C., Grugel, R., Tatje, D., Hoppe, J., Folkman, J., Marme, D. and Weich, H. A. (1992) Basic fibroblast growth factor modulates the mitogenic potency of the platelet-derived growth factor (PDGF) isoforms by specific upregulation of the PDGF alpha receptor in vascular smooth muscle cells. *J. Biol. Chem.* **267**, 18032–18039
- 47 Herbst, J. J., Opresko, L. K., Walsh, B. J., Lauffenburger, D. A. and Wiley, H. S. (1994) Regulation of postendocytotic trafficking of the epidermal growth factor receptor through endosomal retention. *J. Biol. Chem.* **269**, 12865–12873
- 48 McKinley, D. N. and Wiley, H. S. (1988) Reassessment of fluid-phase endocytosis and diacytosis in monolayer cultures of human fibroblasts. *J. Cell Physiol.* **136**, 389–397

Received 22 May 2006/14 November 2006; accepted 22 November 2006

Published as BJ Immediate Publication 22 November 2006, doi:10.1042/BJ20060756

SUPPLEMENTAL RESULTS

MODEL SIMPLIFICATION

At sufficiently low cell densities initial conditions 12 imply, that all terms proportional to the concentration of free extracellular ligand can be safely neglected in Eqs. 2-5 [1] to obtain

$$dL_o / dt \approx k_r (n/N_A) C_s, \quad (S1)$$

$$dC_s / dt \approx -(k_r + k_t) C_s + k_x C_i, \quad (S2)$$

$$dC_i / dt \approx k_t C_s + k_f' (R_{i0} - C_i) L_i - (k_r' + k_x + k_{hr}) C_i, \quad (S3)$$

$$(V_e N_A) dL_i / dt \approx -k_f' (R_{i0} - C_i) L_i + k_r' C_i - k_{hl} (V_e N_A) L_i. \quad (S4)$$

Numerical tests using the base line parameters listed in Tables 1-2 illustrate that this neglect is justified for cell densities up to 10^{10} cells/l (not shown). Furthermore, initial conditions 12 imply that $k_t C_s \ll k_x C_i$, at sufficiently short times. Neglecting the term $k_t C_s$ in Eq. S3 and introducing the *total* number of intracellular ligand molecules per cell, ℓ_i , we obtain the autonomous nonlinear system

$$dC_i / dt \approx k_1 (C_i - C_-[\ell_i])(C_i - C_+[\ell_i]), \quad (S5)$$

$$d\ell_i / dt \approx -(k_x + k_{hr}) C_i - k_{hl} (\ell_i - C_i) \quad (S6)$$

where

$$k_1 \equiv k_f' / (N_A V_e), \quad (S7a)$$

$$K_M \equiv (k_r' + k_x + k_{hr}) / k_1 \quad (S7b)$$

and

$$C_+[\ell_i] \equiv \frac{(R_{i0} + K_M + \ell_i) + ((R_{i0} + K_M + \ell_i)^2 - 4R_{i0}\ell_i)^{1/2}}{2}, \quad (S8a)$$

$$C_-[\ell_i] \equiv \frac{(R_{i0} + K_M + \ell_i) - ((R_{i0} + K_M + \ell_i)^2 - 4R_{i0}\ell_i)^{1/2}}{2} \quad (S8b)$$

are the roots of the quadratic equation

$$C_i^2 - (R_{i0} + K_M + \ell_i) C_i + R_{i0} \ell_i = 0.$$

Eqs. S5-S6 are similar to the equations of enzyme kinetics [2] and can be similarly analyzed using the total quasi-steady state approximation [2,3]. Indeed, Eqs. S5 and S8a,b are formally the same as the equations for the enzyme-substrate complex in irreversible Michaelis-Menten kinetics, with R_{i0} and ℓ_i playing the respective roles of total enzyme and substrate concentrations [2].

THE TOTAL QUASI-STEADY-STATE APPROXIMATION

Initial conditions 12 imply that during the initial transient we can substitute $\ell_i = \ell_{i^*}$ into Eq. S5 to obtain

$$dC_i / dt \approx k_1 (C_i - C_-[\ell_{i^*}]) (C_i - C_+[\ell_{i^*}]). \quad (\text{S9})$$

The solution of this Riccati equation is

$$C_{i,\text{ITA}} = \frac{C_-[\ell_{i^*}](C_+[\ell_{i^*}] - C_{i^*}) + C_+[\ell_{i^*}](C_{i^*} - C_-[\ell_{i^*}])e^{-t/t_C}}{(C_+[\ell_{i^*}] - C_{i^*}) + (C_{i^*} - C_-[\ell_{i^*}])e^{-t/t_C}}, \quad (\text{S10})$$

where

$$t_C^{-1} \equiv k_1 (C_+[\ell_{i^*}] - C_-[\ell_{i^*}]) = k_1 \left((R_{i0} + K_M + \ell_{i^*})^2 - 4R_{i0}\ell_{i^*} \right)^{1/2}. \quad (\text{S11})$$

Self consistency requires that the fractional decrease of $\ell_i(t)$ during the initial transient should be small [2]

$$\varepsilon \equiv (\ell_{i^*} - \ell_i(t_C)) / \ell_{i^*} \ll 1. \quad (\text{S12})$$

Using Eq. S6 to effect a first order McLaurin expansion of $\ell_i(t_C)$ and noting that

$0 \leq C_{i^*} / \ell_{i^*} \leq 1$ we find

$$\varepsilon \approx [(k_x + k_{hr})C_{i^*} / \ell_{i^*} + k_{hl}(1 - C_{i^*} / \ell_{i^*})]t_C \leq (k_x + k_{hr} + k_{hl})t_C. \quad (\text{S13})$$

This entails that the validity of the initial transient approximation is guaranteed by the condition

$$(k_x + k_{hr} + k_{hl})t_C \ll 1. \quad (\text{S14})$$

It is noteworthy that the baseline estimates listed in Tables 1 and 2 satisfy inequality S14. A more detailed analysis of the validity of inequality S14 is given in a subsequent section.

Eq. S10 implies that $C_i(t)$ decreases and in a time of order t_c approaches the minimal asymptotic value implied by the initial conditions, $C_-[\ell_{i^*}]$, which signals the onset of a quasi-steady state (QSS) such that

$$C \approx C_-[\ell_i], \quad t > t_c \quad (\text{S15})$$

$$d\ell_i / dt \approx -(k_x + k_{hr})C_-[\ell_i] - k_{hl}(\ell_i - C_-[\ell_i]) \quad t \geq t_c. \quad (\text{S16})$$

Inequality S12 warrants that Eq. S16 can be solved subject to the initial condition

$$\ell_i = \ell_{i^*}, \quad t = t_c. \quad (\text{S17})$$

Equations S16-S17 imply that the QSS time scale is [2]

$$t_\ell \approx \frac{\ell_{i^*}}{(k_x + k_{hr})C_-[\ell_{i^*}] + k_{hl}(\ell_{i^*} - C_-[\ell_{i^*}])}, \quad (\text{S18})$$

so that the ratio of time scale of the induction period prior to the QSS, t_c , to the QSS time scale is approximately

$$t_c / t_\ell \approx [(k_x + k_{hr})(C_-[\ell_{i^*}] / \ell_{i^*}) + k_{hl}(1 - C_-[\ell_{i^*}] / \ell_{i^*})] t_c \approx \varepsilon. \quad (\text{S19})$$

Inequality S14 therefore guarantees the validity of Eq. S16 even prior to steady state, $t \leq t_c$, thereby justifying the solution of this equation subject to the true initial conditions (Eq. 14).

Moreover, these results can be used to obtain corresponding estimates for free extracellular ligand (Eq. S1) and surface bound ligand (Eq. S2). Since the transient phase ends before significant sorting occurs, only the steady-state value of the internalized complex enters the estimates of surface complex

$$C_s \approx k_x e^{-(k_r+k_i)t} \int_0^t C_i(s) e^{(k_r+k_i)s} ds \approx k_x e^{-(k_r+k_i)t} \int_0^t C_-[\ell_i(s)] e^{(k_r+k_i)s} ds, \quad (\text{S20})$$

and degraded ligand in the medium

$$dL_{\text{deg}} / dt = (n / N_A)(k_{hr}C_i + k_{hl}(\ell_i - C_i)) \approx (n / N_A)(k_{hr}C_-[\ell_i] + k_{hl}(\ell_i - C_-[\ell_i])). \quad (\text{S21})$$

VALIDITY OF THE TOTAL QUASI-STEADY STATE APPROXIMATION

Rewriting S11 in the expanded form

$$t_c^{-1} = k_1(K_M^2 + 2K_M(R_{i0} + \ell_{i^*}) + (R_{i0} - \ell_{i^*})^2)^{1/2} \quad (\text{S22})$$

illustrates that t_C is a bounded function in the (ℓ_{i^*}, R_{i0}) plane and since it is continuous has a maximum in any closed set $\mathbb{R} \times \mathbb{R}$. The partial derivatives are

$$\frac{\partial t_C}{\partial R_{i0}} = -\frac{K_M + (R_{i0} - \ell_{i^*})}{k_1 \left(K_M^2 + 2K_M(R_{i0} + \ell_{i^*}) + (R_{i0} - \ell_{i^*})^2 \right)^{3/2}} \quad (\text{S23})$$

and

$$\frac{\partial t_C}{\partial \ell_{i^*}} = -\frac{K_M - (R_{i0} - \ell_{i^*})}{k_1 \left(K_M^2 + 2K_M(R_{i0} + \ell_{i^*}) + (R_{i0} - \ell_{i^*})^2 \right)^{3/2}}. \quad (\text{S24})$$

The conditions for extrema are therefore

$$K_M + (R_{i0} - \ell_{i^*}) = 0 \quad (\text{S25})$$

and

$$K_M - (R_{i0} - \ell_{i^*}) = 0. \quad (\text{S26})$$

This has no solution, implying that the maximum is on the boundary. It is easy to verify that the maximum is attained at $R_{i0} = \ell_{i^*} = 0$. Thus,

$$t_C(\ell_{i^*}, R_{i0}) \leq t_C(0,0) = (k_r' + k_x + k_{hr})^{-1} \quad (\text{S27})$$

and inequality S12 is guaranteed by the purely kinetic criterion

$$\mu \equiv (k_x + k_{hr} + k_{hl}) t_C(0,0) = \frac{k_x + k_{hr} + k_{hl}}{k_r' + k_x + k_{hr}} \ll 1, \quad (\text{S28})$$

which is valid whenever dissociation of endosomal complex is much faster than the elimination of internalized ligand by degradation and recycling. Moreover, inequality S14 can also be satisfied even when $\mu = O(1)$, provided that $\tau \equiv t_C(\ell_{i^*}, R_{i0}) / t_C(0,0) \ll 1$. The later inequality is valid for a wide range of initial ligand loading and endosomal receptor numbers (Figure S1).

APPROXIMATE LIGAND TIME-COURSE CURVES

The complexity of Eq. S8b does not allow for an explicit closed form solution of the total quasi-steady state rate equation (Eq.S16). To that end we now proceed to simplify the quasi-steady state concentration of endosomal complex (Eq. S8b) in zones I-III ad defined by inequalities 20-23 (Figure 4).

Zone I

Inequality 20 implies that [2]

$$C_-[\ell_i] \approx \frac{R_{i0}\ell_i}{K_M + \ell_i} \ll \ell_i, \quad (\text{S29})$$

$$t_C^{-1} \approx k_1(\ell_{i^*} + K_M). \quad (\text{S30})$$

Substituting S29 into S16 yields

$$d\ell_i / dt \approx -(k_x + k_{hr})C_-[\ell_i] - k_{hl}\ell_i = -\frac{k_\ell\ell_i + k_{hl}\ell_i^2}{\ell_i + K_M}, \quad (\text{S31})$$

where

$$k_\ell \equiv (k_x + k_{hr})R_{i0} + k_{hl}K_M. \quad (\text{S32})$$

When $\ell_{i^*} \ll K_M$, inequality 20 reduces to the $K_M \gg R_{i0}$ limit of inequality 21, studied below. When $\ell_{i^*} \gg K_M + R_{i0}$, inequality 20 reduces to inequality 23, also studied below.

The unique limit of inequality 20 is defined by $\ell_{i^*} \approx K_M \gg R_{i0}$, in which case S31 cannot be integrated explicitly. However, we can approximate the initial apparent dynamics by linearizing the tQSSA results around the initial condition $\ell_i = \ell_{i^*}$. Linearizing S31

$$d\ell_i / dt \approx -\ell_i / t_I, \quad t_I \equiv \frac{\ell_{i^*} + K_M}{k_\ell + k_{hl}\ell_{i^*}}, \quad (\text{S33})$$

and integrating we find

$$\ell_i \approx \ell_{i^*} e^{-t/t_I}. \quad (\text{S34})$$

Linearization of S29 yields

$$C_-[\ell_i] \approx \frac{R_{i0}\ell_i}{K_M + \ell_{i^*}} \approx \left(\frac{R_{i0}\ell_{i^*}}{K_M + \ell_{i^*}} \right) e^{-t/t_I}. \quad (\text{S35})$$

Substituting S35 into S20 and S21 we find, respectively

$$C_s \approx \frac{k_x C_-[\ell_{i^*}](e^{-t/t_I} - e^{-(k_r+k_t)t})}{k_r + k_t - t_I^{-1}}, \quad (\text{S36})$$

and

$$\frac{dL_{\text{deg}} / dt}{(n/N_A)} \approx \left(\frac{k_{hr}R_{i0} + k_{hl}(\ell_{i^*} + K_M)}{\ell_{i^*} + K_M} \right) \ell_{i^*} e^{-t/t_I} \approx k_{hl}\ell_{i^*} e^{-t/t_I}$$

with the solution

$$\frac{L_{\text{deg}}}{(n/N_A)\ell_{i^*}} \approx k_{hl}t_I(1 - e^{-t/t_I}). \quad (\text{S37})$$

Substituting S36 into S1 yields

$$\frac{L_o}{(n/N_A)\ell_{i^*}} \approx \frac{k_r k_x R_{i0}}{(\ell_{i^*} + K_M)(k_r + k_t - t_I^{-1})} \left(\frac{1 - e^{-t/t_I}}{t_I^{-1}} - \frac{1 - e^{-(k_r+k_t)t}}{k_r + k_t} \right). \quad (\text{S38})$$

Zone II

Inequality 21 implies that [2]

$$C_-[\ell_i] \approx \frac{R_{i0}\ell_i}{K_M + R_{i0}}, \quad (\text{S39})$$

$$t_C^{-1} \approx k_1(R_{i0} + K_M). \quad (\text{S40})$$

Substituting S39 into S16 yields

$$d\ell_i / dt \approx -t_R^{-1}\ell_i, \quad t_R \equiv (K_M + R_{i0})/k_\ell \quad (\text{S41})$$

with the solution

$$\ell_i \approx \ell_{i^*} e^{-t/t_R}. \quad (\text{S42})$$

Substituting S39 and S42 into Eqs. S20-S21 yields, respectively

$$C_s \approx \frac{k_x C_-[\ell_{i^*}](e^{-t/t_R} - e^{-(k_r+k_t)t})}{k_r + k_t - t_R^{-1}} \quad (\text{S43})$$

and

$$dL_{\text{deg}} / dt \approx (n/N_A) \left(\frac{k_{hr}R_{i0} + k_{hl}K_M}{R_{i0} + K_M} \right) \ell_{i^*} e^{-t/t_R}$$

with the solution

$$\frac{L_{\text{deg}}}{(n/N_A)\ell_{i^*}} \approx \left(\frac{k_{hr}R_{i0} + k_{hl}K_M}{R_{i0} + K_M} \right) t_R (1 - e^{-t/t_R}). \quad (\text{S44})$$

Substituting S43 into S1 yields

$$\frac{L_o}{(n/N_A)\ell_{i^*}} \approx \frac{k_r k_x R_{i0}}{(R_{i0} + K_M)(k_r + k_t - t_R^{-1})} \left(\frac{1 - e^{-t/t_R}}{t_R^{-1}} - \frac{1 - e^{-(k_r+k_t)t}}{k_r + k_t} \right). \quad (\text{S45})$$

Zone III

Inequality 22 implies that [3]

$$C_-[\ell_i] \approx \ell_i, \quad (\text{S46})$$

$$t_C^{-1} \approx k_1(R_{i0} - \ell_{i^*}). \quad (\text{S47})$$

Substituting S46 into S16 yields

$$d\ell_i / dt \approx -(k_x + k_{hr})\ell_i$$

with the solution

$$\ell_i \approx \ell_{i^*} e^{-(k_x + k_{hr})t}. \quad (\text{S48})$$

Substituting S46 and S48 into Eqs. S20-S21 yields, respectively

$$C_s \approx \frac{k_x \ell_{i^*} (e^{-(k_x + k_{hr})t} - e^{-(k_r + k_t)t})}{k_r + k_t - (k_x + k_{hr})} \quad (\text{S49})$$

and

$$dL_{\text{deg}} / dt \approx (n / N_A) k_{hr} \ell_i \approx (n / N_A) k_{hr} \ell_{i^*} e^{-(k_x + k_{hr})t}$$

with the solution

$$\frac{L_{\text{deg}}}{(n / N_A) \ell_{i^*}} \approx \frac{k_{hr}}{k_x + k_{hr}} (1 - e^{-(k_x + k_{hr})t}). \quad (\text{S50})$$

Substituting result S49 into S1 yields

$$\frac{L_o}{\ell_{i^*} (n / N_A)} \approx \frac{k_r k_x}{k_r + k_t - (k_x + k_{hr})} \left(\frac{1 - e^{-(k_x + k_{hr})t}}{k_x + k_{hr}} - \frac{1 - e^{-(k_r + k_t)t}}{k_r + k_t} \right). \quad (\text{S51})$$

Zone IV

Inequality 23 implies that [3]

$$C_-[\ell_{i^*}] \approx R_{i0}, \quad (\text{S52})$$

$$t_C^{-1} \approx k_1(\ell_{i^*} - R_{i0}). \quad (\text{S53})$$

Substituting S52 into S16 yields

$$\dot{\ell}_i \approx (k_{hl} - (k_x + k_{hr}))R_{i0} - k_{hl}\ell_i$$

with the solution

$$\ell_i \approx \left(\ell_{i^*} + \left(1 - \frac{k_x + k_{hr}}{k_{hl}} \right) R_{i0} \right) e^{-k_{hl}t} + \left(1 - \frac{k_x + k_{hr}}{k_{hl}} \right) R_{i0}. \quad (\text{S54})$$

This equation is only valid while ℓ_i satisfies inequality 23 and $C_i \approx R_{i0}$. Eventually $\ell_i \approx K_M + R_{i0}$ and the approximation breaks down.

ON THE RATIO R_{i0} / K_M

It is straightforward to verify that Eq. 16 is equivalent to the hyperbolic relationship

$$C_i = \frac{R_{i0}(\ell_i - C_i)}{K_M + (\ell_i - C_i)} = \frac{R_{i0}N_A V_e L_i}{K_M + N_A V_e L_i}. \quad (\text{S55})$$

Eq. S55 implies that K_M corresponds to the free ligand number for which half of the binding sites are saturated, $C_i = R_{i0} / 2$ and $C_i / \ell_i = R_{i0} / (R_{i0} + 2K_M)$. Thus, the fraction of ligand that is bound at half saturation increases with the ratio R_{i0} / K_M . For a general ligand concentration $(N_A V_e)L_i = \alpha K_M$ and $C_i / \ell_i = R_{i0} / (R_{i0} + (\alpha + 1)K_M)$, directly illustrating that the fraction of bound ligand always increases with the ratio R_{i0} / K_M and tends to unity as $R_{i0} / K_M \rightarrow \infty$.

INTERNALIZATION KINETICS IMPACT ENDOSOMAL STABILITY

Following [4] we replace the dynamical model of surface kinetics and internalization by a constant prescribed flux of growth factor-receptor complex,

$$C_s \approx R_{s0} L_0 / (K_d + L_0). \quad (\text{S56})$$

This reduces our model to

$$\dot{C}_i = k_e C_s + k_f' R_i L_i - k_r' C_i - (k_{hr} + k_x) C_i, \quad (\text{S57})$$

$$(V_e N_{av}) \dot{L}_i = -k_f' R_i L_i + k_r' C_i - k_{hl} (V_e N_{av}) L_i. \quad (\text{S58})$$

$$\dot{R}_i = -k_f' R_i L_i + k_r' C_i - (k_{hr} + k_x) R_i. \quad (\text{S59})$$

Note that this reduced model neglects the internalization of free receptors, and therefore underestimates the number of endosomal receptors. As predicted by our analysis the reduced model underestimation the stability of endosomal ligand (Figure S.2).

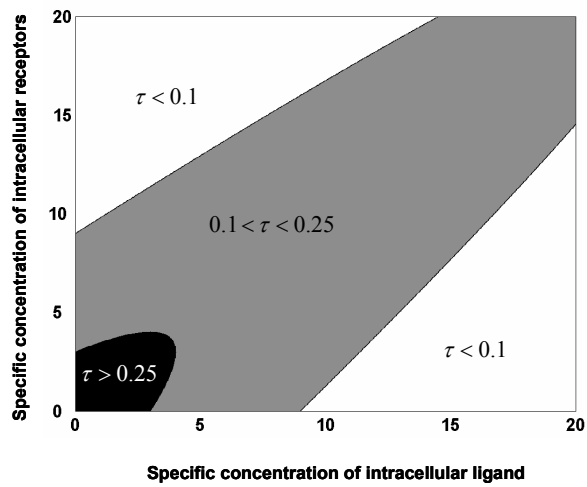


Figure S1 Normalized binding time scale $\tau \equiv t_C(\ell_{i^*}/K_M, R_{i0}/K_M)/t_C(0,0)$ as a function of specific endosomal ligand ℓ_{i^*}/K_M and receptor R_{i0}/K_M concentrations. Color code: (White) $\tau \leq 0.1$, (gray) $0.1 \leq \tau \leq 0.25$ and (black) $0.25 < \tau \leq 1$.

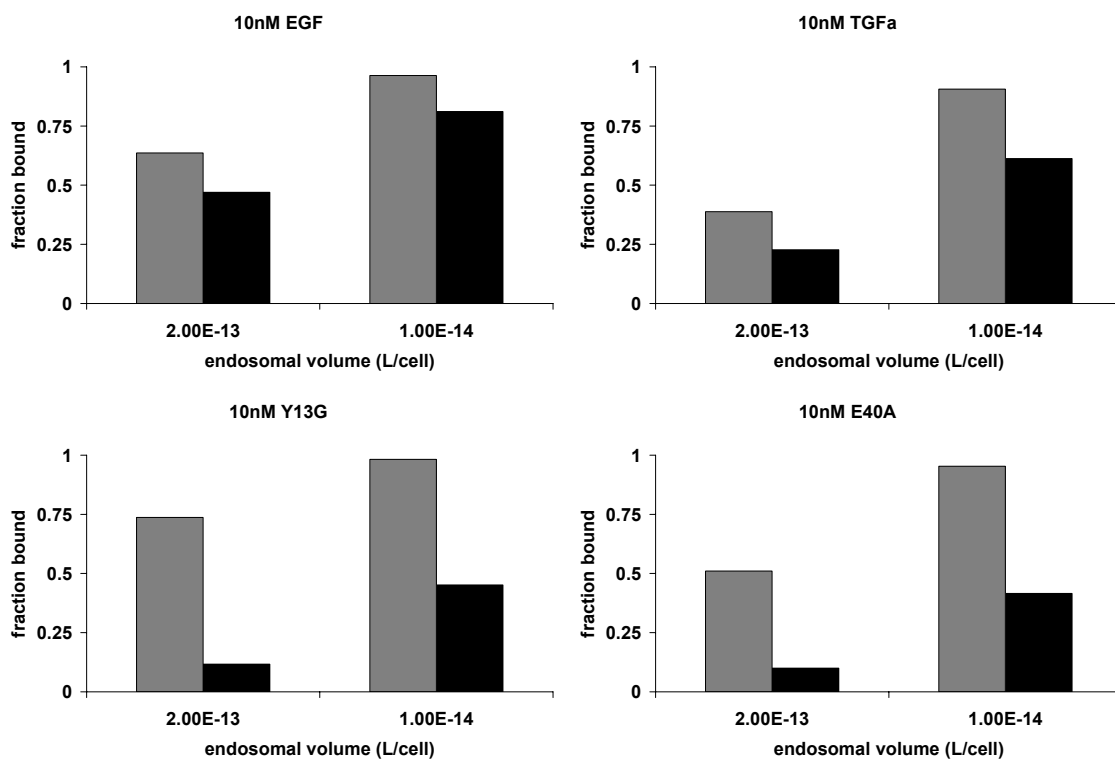


Figure S2 Fraction of bound endosomal ligand at the end of 180 minute incubations with 10nM of EGF, TGF α , Y13G or E40A. (Grey) Eqs. 1-6, (black) Eqs. S56-S59. Both sets of simulations employ the parameter values listed in Tables 1-2.

REFERENCES

1. Tzafirri, A. R., Wu, D. and Edelman, E. R. (2004) Analysis of compartmental models of ligand-induced endocytosis. *J. Theor. Biol.* **229**, 127-138.
2. Tzafirri, A. R. (2003) Michaelis-Menten kinetics at high enzyme concentrations. *Bull Math Biol.* **65**, 1111-29.
3. Tzafirri, A. R. and Edelman, E. R. (submitted) Quasi-steady state kinetics at enzyme and substrate concentrations in excess of the Michaelis-Menten constant.
4. French, A. R. and Lauffenburger, D. A.(1996) Intracellular receptor/ligand sorting based on endosomal retention components. *Biotech. Bioeng.* **51**, 281-297.